Studying Cloud Structure on Venus with VIRTIS

J. K. Barstow

August 25, 2010

Second Year Report

Supervisor: Professor F. Taylor

Lady Margaret Hall

Atmospheric, Oceanic and Planetary Physics, University of Oxford

$\sim$ 13000 words

Abstract

Near-infrared spectra from the Visible and Infrared Thermal Imaging Spectrometer (VIRTIS) on Venus Express provide the opportunity to investigate a wide range of Venusian atmospheric parameters. The sulphuric acid clouds are of particular interest, since they significantly affect the radiative budget of the planet on a range of spatial scales, but are not yet well-understood. Determination of gaseous abundances by comparisons between radiative transfer model spectra and data is heavily dependent on the rep-resentation of the cloud in the model, so an improved understanding of the cloud structure is crucial for the study of the Venusian lower atmosphere.

VIRTIS-M-IR, the infrared section of the VIRTIS mapping specrometer, is used in this work. Models were produced using the NEMESIS radiative transfer and retrieval code (Irwin et al. 2008). The spectral window regions covered by VIRTIS-M-IR are sensitive on the nightside of the planet to absorption by the lower and middle cloud layers, which are back-lit by radiation from the the hot lower atmosphere and surface. Variable input quantities in the cloud model, apart from the total lower cloud optical depth, are the concentration of the acid in the clouds, the average size of the particles (altered by varying the relative abundances of the mode $2'$ and larger mode 3 particles) and the vertical distribution of the cloud (parameterised by varying the altitude of the cloud base). The sensitivity to these variables across the VIRTISM-IR spectral range can be explored by comparing radiances at pairs of wavelengths in model branch plots and thereby defining a parameter space sensitive to one or more of these variables. Using multiple branch plots allows the variation due to each of these variables to be independently characterised. The position of each data point in such a parameter space can then be used to infer values for acid concentration, the abundance of mode 3 particles and cloud base altitude.

This technique allows the spatial variation of sulphuric acid concentration in the Venusian cloud particles to be estimated for the first time. Since the form of the infrared spectrum is heavily dependent on this acid concentration, constraining the concentration is a crucial first step in the determination of other cloud properties and gaseous abundances by remote sounding techniques.

Contents

List of Tables

List of Figures

1 Introduction

1.1 The Planet Venus

Venus is a rocky planet of approximately the same size as the Earth, orbiting the Sun at ∼0.72 of the Earth's orbital radius. It has an orbital period of 224 days, and a retrograde rotation with a period of 243 days. This slow rotation results in atmospheric dynamics very different to those on the Earth.

The estimated surface temperature of a Venus in radiative equilibrium with incoming solar radiation would be ∼240 K, slightly cooler than that of the Earth. However, Venus has a massive atmosphere with a surface pressure of 90 bars, and the atmosphere is composed primarily of carbon dioxide which is highly absorbing in the infrared, creating an efficient greenhouse effect. The resulting average surface temperature is closer to 740 K.

Venus is covered in a layer of cloud from ∼48–75 km. This cloud is thought to be composed of concentrated sulphuric acid droplets, although the precise composition is still uncertain. The cloud layer contributes to the extremely high bolometric albedo of Venus, which is ∼0.7. Ultraviolet features indicate the presence of an ultraviolet absorber, thought to be present at the same altitude as the cloud top. However, so far all attempts to identify the substance responsible have been unsuccessful.

The slow rotation of Venus results in an atmospheric super-rotation. Zonal wind speeds in the troposphere and mesosphere of up to 90 ms^{-1} have been recently inferred from the temperature field as measured by the Visible and Infrared Thermal Imaging Spectrometer (VIRTIS) on Venus Express by Piccialli et al. (2008). The mechanism for this super-rotation is still not understood. Above 100 km, solar heating creates a strong diurnal temperature gradient which results in a strong sub-solar – anti-solar flow. Meridional transport is dominated by a Hadley cell between the equator and ∼50° latitude. The meridional extent of the Hadley cell has been inferred from an observed decrease in cloud top altitude at ∼50° (Titov et al. 2008). This conclusion is supported by the observed increase in the concentration of carbon monoxide at 35 km altitude and ∼60° latitude, caused by a downward transport of CO-rich air with the downwelling branch of the Hadley cell (Tsang et al. 2008b).

Atmospheric vortices that are most often dipolar in shape have been observed close to both poles, and these are thought to be driven by the meridional Hadley cell transport. They are characterised by infrared-bright double-eye features (Piccioni et al. 2007). The shape of these vortices has been observed to vary between observations, and the exact mechanism for their formation is poorly understood. Similar vortices on Titan are thought

to act as a mixing barrier in the stratosphere and mesosphere (Teanby et al. 2008), and it is possible that such considerations apply on Venus.

Venus has a much higher abundance of CO_2, CO and SO_2 than the Earth, but its atmosphere is much drier. A comparison is provided below in Table 1, with values taken from Taylor & Grinspoon (2009). The reasons for these compositional differences are unclear, particularly if the initial atmospheres of Earth and Venus were identical in composition, but it is thought that the relatively high abundance of SO_2 is due to high levels of volcanic activity. Donahue et al. (1982) interpret the high deuterium-hydrogen abundance ratio as measured by the Pioneer Venus large probe mass spectrometer as evidence that Venus was once much wetter than it is today. The low abundance of atmospheric CO_2 on Earth compared to that of Venus could be explained by the high uptake of CO_2 by the oceans on Earth and the subsequent formation of carbonate minerals.

	Venus	Earth
CO_2	0.96	0.003
N_2	0.035	0.770
Atomic O	trace	trace
H_2O	0.000030	$\sim$0.01
SO_2	0.00015	0.2 ppb
CO	0.00004	0.12 ppm
Surface Pressure	92 bar	1 bar
Surface Temperature	$\sim$740 K	$\sim$290 K

Table 1: A comparison table for the atmospheres of Earth and Venus. Abundances are taken from Taylor & Grinspoon (2009), and are given as fractions unless otherwise specified.

Venus has the greatest number of 'volcanic' topographic features in the solar system, and areas of high surface emissivity have also been interpreted as evidence of lava flows. Radar-bright features from ground-based measurements were interpreted as volcanic in origin by Saunders & Malin (1977), and the topographical maps generated using data from the Magellan probe have provided evidence that over 90% of the surface is covered by features that bear a close resemblance to volcanic features on Earth (Head et al. 1992). With data from VIRTIS, correlations between high emissivity regions and volcanic features interpreted from Magellan topography data have been observed (Helbert et al. 2008). Whereas the presence of past volcanism on Venus is widely accepted, it is unknown whether it occurred continuously or in sporadic bursts of high activity. Esposito et al. (1988) suggest that

an observed decrease in sulphur dioxide concentration above the cloud tops during the Pioneer Venus mission could be evidence that volcanic activity has occurred more recently, possibly favouring a more constant outgassing model.

Venus has no significant intrinsic magnetic field, so the solar wind interacts directly with the upper atmosphere. The MAG and ASPERA instruments on Venus Express will be used to investigate this interaction and the Venus plasma environment during the mission (Zhang et al. 2006).

1.2 Venus Express

Venus Express (VEX) was launched in November 2005 and entered orbot around Venus in April 2006. The nominal mission was due to last for 2 Venus sidereal days, but has now been extended until December 2012 to overlap with the Japanese Akatsuki Venus mission. Seven science instruments are onboard VEX. These are the Analyser of Space Plasma and Energetic Atoms (ASPERA), a magnetometer (MAG), the Planetary Fourier Spectrometer (PFS, not useable due a a scanning fault), SPectroscopy for Investigation of Characteristics of the Atmosphere of Venus and Solar Occultaion in the InfraRed (SPICAV/SOIR), the Venus Radio Science Package (VeRa), the Visible and InfraRed Thermal Imaging Spectrometer (VIRTIS), and the Venus Monitoring Camera (VMC). Data from VIRTIS have been used in this work and the instrument is described below in more detail.

1.3 The Visible and Infrared Thermal Imaging Spectrometer

VIRTIS was originally designed for the cometary mission Rosetta, to study the mineralogy and petrology of the comet P\Wirtanen (Coradini et al. 1998). It consists of three unique data channels, two of which are mapping channels, one operating in the wavelength range 0.25–1.0 μm (VIRTISM-VIS) and the other in the range 1.0–5.0 μm (VIRTISM-IR). The spectral sampling of VIRTIS-M is 0.01 μm. The third channel is devoted to spectroscopy, and is a high-resolution echelle spectrometer operating in the range 2.0–5.0 μm (VIRTIS-H). The work presented here uses data from the VIRTISM-IR channel. A schematic of the instrument taken from Coradini et al. (1999) is shown in Figure 1.

Data from the VIRTIS-M part of the instrument are transmitted as a three-dimensional cube, with two spatial dimensions and one spectral dimension. The spectrometer slit is 256 pixels across, and during each observation

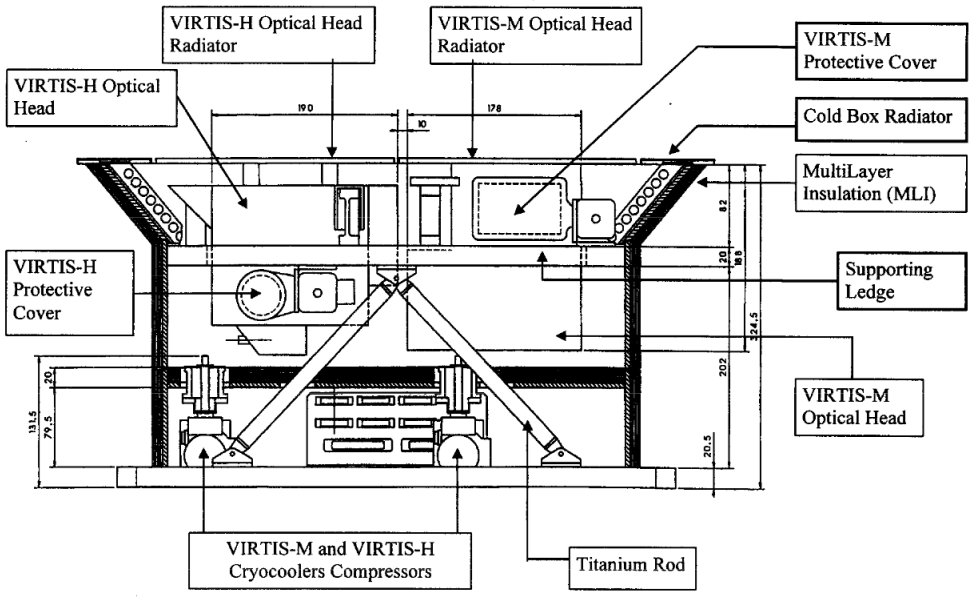

Figure 1: A schematic of the VIRTIS optics module, taken from Coradini et al. (1999).

VIRTIS-M scans in a direction perpendicular to the orientation of the slit, recording a 256×256 pixel image. The third dimension of the cube is provided by the 432 spectral channels (Drossart et al. 2007). Geometry files are also distributed with the calibrated data, which contain geometrical data for each individual pixel. The instantaneous field of view of VIRTIS-M over the whole slit is 0.25×64 mrad, which corresponds to a distance of ∼1/3 of the diameter of the planet at apocentre. After taking into account scanning by the secondary mirror, the total field of view is 64 mrad (Drossart et al. 2007). The spectral resolution of VIRTIS-M is given by Svedhem et al. (2007) as $(\lambda/\Delta\lambda)$ ∼200, and the size of a single pixel is 0.25 mrad. This corresponds to a spatial resolution of ∼20 km even at apocentre (60,000 km from the planet).

2 Radiative Transfer Models

Nemesis, the Non-linear optimal Estimator for MultivariatE spectral analySIS (Irwin et al. 2008), was created as a retrieval code that could be used to model any planet and data from any instrument. It uses a non-linear optimal estimator formalism to find the best-fit forward model to a spectrum for up to four different variables simultaneously, allowing the solution of an

under-constrained problem.

Performing a retrieval involves the generation of a radiative transfer model using a set of a priori values for various parameters, and these radiative transfer models will be used in this work. The model spectrum generated may be sensitive to some or all of these parameters in certain wavelength regions. The input for *NEMESIS* for Venus currently uses pressure and temperature values from the models of Seiff et al. (1985) to produce vertical profiles consisting of 111 altitude levels, ranging from the surface to 150 km. Seiff et al. (1985) used data collected by the Pioneer Venus probes and orbiters and Veneras 10, 12 and 13 to obtain optimal model profiles. Gaseous abundance vertical profiles are taken from Kliore et al. (1986), and vertical profiles for four cloud modes as described in Section 3.2 are used. *NEMESIS* calculates the spectral radiance leaving the atmosphere at the required spectral resolution, allowing the calculation of forward models to simulate results from a range of instruments.

Radiative transfer models are calculated by solving the radiative transfer equation (1) for a given set of initial values for each variable parameter:

$$L_\nu = B_\nu(T_0)\tau_\nu(0) + \int_{\tau_\nu(0)}^{1} B_\nu(T)\,\mathrm{d}\tau_\nu(z). \tag{1}$$

In Equation (1), L_ν is the resulting spectral radiance after radiation has passed through an atmosphere from the surface to altitude z. $B_\nu(T_0)$ is the Planck function at surface temperature T_0 and wavenumber ν, $B_\nu(T)$ is the Planck function at temperature T for an altitude z, $\tau_\nu(z)$ is the optical depth at altitude z and $\tau_\nu(0)$ is the total optical depth of the atmosphere. The first term in the equation represents the attenuation of radiation between the surface and altitude z by the intervening atmosphere, and the second term represents radiation emitted by the atmospheric gas or scattered into the beam.

Clearly, the solution to this equation requires knowledge of the strengths and positions of absorption lines for gaseous constituents in the atmosphere. If the gaseous absorption for a wavenumber region $\nu \rightarrow \nu+\Delta\nu$ is calculated by taking into account the exact contribution for each individual absorption line this is very time-consuming, and as several iterations are required before the best-fit model is calculated it is very inefficient. Two possible approximations can reduce computation time significantly: the band model approximation and the correlated-k approximation. The band model approximation cannot be used in a scattering atmosphere, and as the clouds on Venus are strong scatterers in the VIRTIS wavelength range the correlated-k approximation, originally used by Lacis & Oinas (1991), is the preferred option.

The correlated-k approximation assumes that the precise location of an absorption line of absorption coefficient k within a small frequency interval $\nu \rightarrow \nu + \Delta\nu$ is of no importance to the calculation of the transmission in that interval. It is in fact sufficient to know what fraction of the frequency domain $f(k)\mathrm{d}k$ is occupied by absorption coefficients between k and $k + \mathrm{d}k$ (Irwin et al. 1997). Then, the mean transmission within this interval can be described as:

$$\bar{T}(m) = \int_0^\infty f(k)e^{(-km)}\mathrm{d}k \tag{2}$$

where m is the number of molecules per square metre of atmosphere. Equation (2) has the form of a standard Laplace transform of the frequency distribution of k, and it is independent of the ordering of the absorption coefficients. Therefore we can define the cumulative frequency distribution

$$g(k) = \int_0^k f(k)\mathrm{d}k \tag{3}$$

and if Equation (3) is inverted such that $k(g) = g^{-1}(k)$ then we can rewrite $\bar{T}(m)$ as

$$\bar{T}(m) = \int_0^1 e^{(-k(g)m)}\mathrm{d}g. \tag{4}$$

If we divide the space between $g = 0, 1$ into N intervals such that g is well-sampled, we can then express $\bar{T}(m)$ as a sum rather than an integral:

$$\bar{T}(m) = \sum_i^N e^{(-\bar{k}_i m)}\Delta g_i. \tag{5}$$

This is valid for a homogeneous path through an atmosphere. In reality, such paths are inhomogeneous, and this inhomogeneity can be approximated by adding homogeneous layers together. The transmission within each layer is generally well-correlated with the transmissions in adjacent layers, so this approximation is valid. The name 'correlated-k' arises from this fact (Tsang 2007). The distribution $k(g)$ can be calculated and used as an input to the radiative transfer model, resulting in a fast forward model calculation.

Line strength data for common atmospheric gases are obtained from laboratory measurements, although for a planet such as Venus some degree of extrapolation in temperature and pressure is required as the conditions are very different from those on Earth. The correlated-k tables for Venus are created using data from two main databases (Tsang et al. 2008a). These are HITEMP (Rothman et al. 2010) and HITRAN2K (Rothman et al. 2003).

CO_2 values from HITEMP are used, as this database contains weak rotational lines and bands that become important at high temperatures and are absent in HITRAN2K (Tsang 2007). Both Pollack et al. (1993) and Tsang (2007) find that simulations using HITEMP data are much improved over simulations using only HITRAN CO_2 lines. All other gaseous parameters are taken from HITRAN2K.

3 The Venusian Cloud

The clouds on Venus play an extremely important role in the energy balance of the atmosphere, and so understanding them is of vital importance if we are to comprehend the evolution of the Venusian climate. The high albedo (reflectivity) of the clouds prevents much of the solar radiation from penetrating to the surface, and the sulphuric acid aerosol particles that form the clouds are also strong scatterers in the near-infrared and strong absorbers at wavelengths above $\sim$3 μm, contributing to the greenhouse effect by preventing thermal radiation from the surface from escaping into space.

After brightness temperatures derived from microwave observations provided initial evidence that the surface temperature of Venus was at least 600 K (Sagan 1960), Sagan (1962) discussed the possibility of a greenhouse model for Venus, having postulated that water clouds were partially responsible for this effect (Sagan 1960). Evidence of a stronger compositional candidate for the cloud began to emerge a decade later, when Young (1973) summarised the inferred properties of the cloud particles from optical polarisation data. He concluded that the only substance consistent with the available spectroscopic and polarimetric data was concentrated sulphuric acid in liquid droplets, containing about 75% by weight H_2SO_4. Young also pointed out that the presence of sulphuric acid is to be expected on a planet with a high level of volcanic activity, as it is a naturally-occurring constituent of volcanic gas and can also be formed from other outgassed substances (water and SO_2). He concluded that other suggestions such as the acids HCl, HF and HNO_3 could be ruled out, at least as candidates for the upper cloud layer.

This conclusion is supported by the work of Pollack et al. (1974), who also interpreted reflectance spectra in the 1.2–4.1 μm wavelength region as also indicative of a sulphuric acid cloud layer. Pollack et al. compared Venusian reflectance spectra with synthetic spectra for several possible candidates and determined that the only substance that matched a cloud absorption feature between 3 and 4 μm was a solution of H_2SO_4, with a concentration of 75 % by weight or higher. It was, however, not possible to distinguish between solutions of 75 and 95 wt % using these data. The possibility of impurities

being present in the aerosol particles was invoked to explain a poor match between H_2SO_4 synthetic spectra and data in the ultraviolet region of the Venus spectrum.

The Pioneer Venus mission, described in detail by Colin (1980), featured a range of instruments on an orbiter and several descent probes devoted to studying the Venusian cloud. These were the nephelometers on the large and small descent probes (LN/SN), the Large Probe Cloud Particle Size Spectrometer (LCPS) and the Orbiter Cloud PhotoPolarimeter (OCPP). The five descent probes entered the atmosphere at different locations. These consisted of three small probes, one entering the dayside (Day) atmosphere, one the nightside (Night) and the third entering the atmosphere at around 60° latitude in the northern hemisphere (North). A large probe (Sounder) and the bus on which the probes were mounted also entered the atmosphere. The cloud vertical profiles obtained by these probes were generally in good agreement with similar profiles derived from backscattering nephelometer data from the Venera 9, 10, 11, 13 and 14 probes, although some variations in the cloud base and cloud top regions were noticeable (Kliore et al. 1986).

The LCPS instrument provided a vertical profile of the cloud, distinguishing between three different aerosol particle size modes. These modes range from mode 1, the smallest, to mode 3, the largest. Kliore et al. (1986) includes a plot, reproduced below (Figure 2), of the vertical distribution of these three particle modes at the Large Probe descent site.

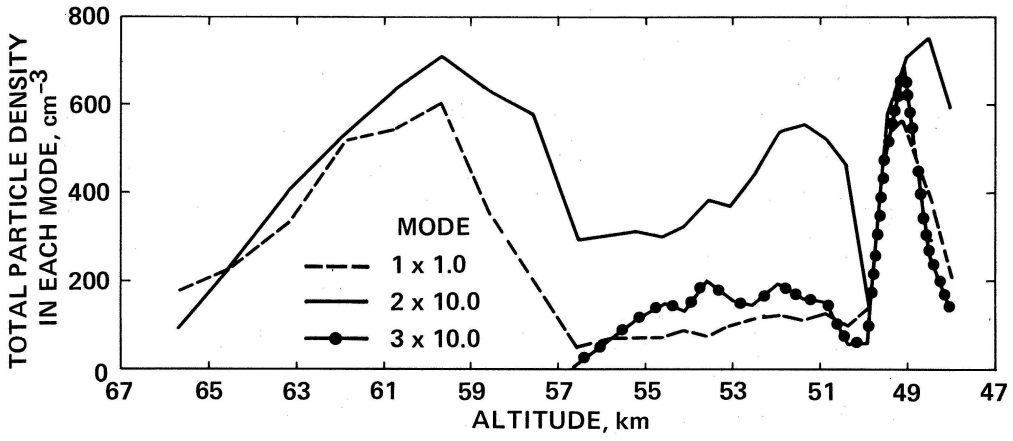

Figure 2: Particle number densities in the three size modes obtained from LCPS data, as presented in Kliore et al. (1986).

The question of possible impurities in the cloud particles was revisited after results from the Pioneer Venus mission became available. Cimino (1982)

examined data from the radio occultation experiment, and modelled the aerosol particles as a solid dielectric sphere with a coating of liquid sulphuric acid. This increases the absorptivity of the particles compared to a pure sulphuric acid sphere. The mass contents derived from the radio occultation data, assuming liquid concentrated H_2SO_4 aerosols, are more than an order of magnitude greater than mass contents determined by the LCPS, which suggested that particles with a higher absorptivity were required. The spectral dependence of the absorption coefficient determined for the occultation data was also found to be different from that of liquid H_2SO_4. She concluded that the best-fit model consisted of a solid core making up 97 % of the particle by radius, with a thin coating of liquid H_2SO_4.

It is now known that the cloud opacity is highly variable, so a cloud mass content observed at one time and in one place could very conceivably differ by an order of magnitude from a content observed elsewhere. However, we cannot yet rule out the possibility of impurities in the cloud particles, especially as the nature of the ultraviolet absorber in the cloud top regions remains unknown. The composition of the largest cloud particles in the lower cloud is also a subject of debate. Esposito et al. (1983) suggested chlorides such as HCl or $FeCl_3$ instead of H_2SO_4, or $NOHSO_4$.

Current observations by VIRTIS allow the study of the Venusian cloud using the infrared window regions discovered by Allen & Crawford (1984) between 1.0 and 2.6 μm. Radiance at these wavelengths is heavily attenuated by the cloud and as such measurements at these radiances provide a good indication of cloud opacity (Figure 3). It has become apparent that alterations in mean particle size and base altitude can also have a significant effect on the measured spectra from Venus (Carlson et al. 1993, Wilson et al. 2008, Satoh et al. 2009). The cloud can also be sounded using the VMC, which monitors the cloud top in the ultraviolet and VeRa, which provides radio occultation profiles of the neutral atmosphere.

3.1 Clouds in Radiative Transfer Models

A detailed cloud model, based on data from the OCPP, LCPS and Solar Flux Radiometer was used by Crisp (1986) in his radiative transfer model of the Venus atmosphere. His cloud model consists of four H_2SO_4 aerosol particle modes, with radii for each mode listed in Table 2. An upper haze is present between 80 and 90 km, the upper cloud above $\sim$ 57 km has a bimodal distribution of mode 1 and mode 2 particles, and the lower cloud from $\sim$ 48–57 km has a trimodal particle distribution of modes 1, 2 and 3 (mode 2′ is treated as a tail of the mode 2 size distribution but is restricted to the middle and lower cloud layer). The ultraviolet absorber is incorporated

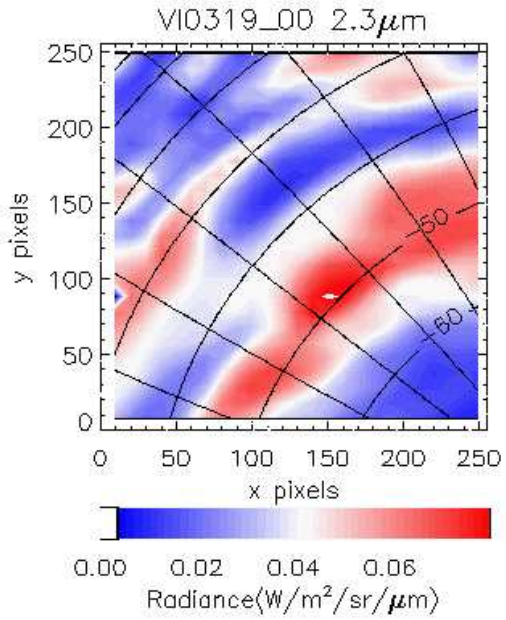

Figure 3: An image of Venus at 2.3 μm, plotted using VIRTISM-IR data from orbit 0319, observation 00. The data have been coadded spatially in bins of 20 × 20 pixels, at 10 pixel intervals. Blue corresponds to thick cloud and low radiance, whilst red indicates thin cloud and high radiance.

into the mode 1 particles in the upper clouds.

Crisp's cloud model is characterised by a lower cloud for which aerosol particle abundance does not decrease noticeably with height, and an upper cloud with a scale height of the same order as the atmospheric scale height. These vertical distributions and size distributions are based on the interpretation of results from the Pioneer Venus OCPP and LCPS experiments, data from both being used to constrain optical depths for the upper cloud and LCPS data being used for the lower cloud.

Mode	Effective Radius at Equator (μm)	Eff. Rad. at Poles (μm)
Mode 1	0.49	0.29
Mode 2	1.18	1.01
Mode 2′	1.40	1.40
Mode 3	3.65	3.65

Table 2: Aerosol particle size distribution as used in the radiative transfer model of Crisp (1986).

This model was further developed by Pollack et al. (1993), incorporating data from the Galileo/NIMS flyby. In their model spectra for the nightside of Venus, mode 2 particles are restricted to the upper cloud only, whilst mode $2'$ and mode 3 are restricted to the lower cloud. Opacity profile modifications were made in order to bring the model into better agreement with the NIMS data.

A similar parameterisation was produced by Grinspoon et al. (1993). They generated a best-fit vertical cloud model by comparing synthetic limb-darkening curves with those obtained from the Galileo/NIMS data. They found that the data were fit best by a model in which the upper cloud optical depth remains constant, and that the majority of the cloud opacity variation occurs in the region from 48–50 km. The results from Grinspoon et al. (1993) and Pollack et al. (1993) are similar, and favour a three- or four-mode cloud model with larger mode 3 particles towards the bottom of the cloud. The nominal cloud base is given in Pollack et al. (1993) as 48 km. Further evidence for a cloud base of $\sim$48 km is provided by the Pioneer Venus descent probe results, as summarised by Kliore et al. (1986), and in Mariner 10 data reanalysed by Kolodner & Steffes (1998).

All three models described above used refractive index data for sulphuric acid obtained from laboratory measurements by Palmer & Williams (1975). These data were used, together with the assumed size distributions, to calculate the extinction coefficient and single scattering albedo for each mode at each wavelength. The derived scattering properties were then included in the radiative transfer model. Grinspoon et al. (1993) used values of 84.5 in the upper cloud and 95.6 wt % H_2SO_4 in the lower cloud, as opposed to the 75 wt % used by Crisp (1986) and Pollack et al. (1993). Palmer & Williams (1975) provide optical data for these three concentrations. Distinguishing between different concentrations of acid using observational data is not straightforward as the problem is underconstrained.

There are other sources of uncertainty for such models. No data were available between the cloud top and the 75 mbar level at the time of Crisp's model, mode 1 particles were too small to be detected by the LCPS instrument, and the extrapolation of a model based on descent probe data to a planet-wide scale is based on the potentially flawed assumption that the conditions at the probe entry site and time were typical. However, the Galileo/NIMS data provided an opportunity to refine this model using remote-sounding data obtained over a wider area of the planet, and went some way towards removing these uncertainties. The Crisp model as refined by Pollack et al. (1993) and the model of Grinspoon et al. (1993) together gave the most accurate representation of the Venusian cloud that was possible with the data available at the time, showing significant agreement despite

different approaches, and therefore these models have been used as a starting point for those developed in this work.

New possibilities were opened up with the data obtained by Venus Express. Satoh et al. (2009) postulate that there may be small haze particles as low in the atmosphere as 30 km, based on a best-fit forward model of the shape of the 1.74 μm peak, but if so these particles cannot be made of concentrated sulphuric acid as sulphuric acid vapour is expected to decompose into SO_3 and H_2O at temperatures found below 45 km altitude on Venus (Prinn 1978). The possibility of alterations in the average particle size across the planet is explored by Wilson et al. (2008), after initial findings by Carlson et al. (1993). They find that the ratio of the peak radiances at 1.74 and 2.3 μm is indicative of a 'size parameter' for a cloud model with a single-mode size distribution. When the results of this model are compared with VIRTISM-IR data, they find that the average particle size is constant over most of the planet but increases towards the poles, indicating that cloud formation processes are different at latitudes greater than 60°, possibly as a result of a different convective regime. Erard et al. (2009) suggest that their independent component analysis of VIRTIS spectra indicates variation in particle size within the polar region, with regions of different average particle size forming concentric rings around the polar vortex.

3.2 The Current A Priori Cloud Model

The current model uses the same a priori optical depths and cloud top altitudes as Pollack et al. (1993). However, the fractional scale heights have been increased from the profile suggested by Pollack, to $1 \times H_{atm}$ in the upper cloud and $4 \times H_{atm}$ in the lower cloud. This removes cloud particles from the line-forming region in the lower cloud whilst maintaining the required optical depth, which corrects for some spectral distortion observed between 2.3 and 2.5 m in models with high cloud optical depths. It also brings the distribution of particles in the model closer to that suggested by Crisp (1986), particularly in the lower cloud, and reflects the mostly-uniform distribution with altitude seen by the Pioneer Venus and Venera descent probes. A best-fit a priori base altitude was determined by fitting models to several ratios of the 2.3 m window spectra from pixels of different radiances (Tsang et al. 2010, in preparation). This indicates the variation in the cloud absorption over that spectral window, and that this variation is sensitive to the altitude of the cloud base. The a priori base altitude we obtain is similar to that given in Pollack et al. (1993), and is 45 km. The a priori cloud particle distributions are shown in Figure 4, and for comparison the results from Pollack et al. (1993) are shown in Figure 5.

Refractive index data for sulphuric acid are taken from Palmer & Williams (1975). Particles with 75% sulphuric acid are initially taken to be the a priori case. The size distribution used is given in Table 3 and is based on that used in Pollack et al. (1993).

Mode	Effective Radius (μm)	Variance (μm)
Mode 1	0.30	0.44
Mode 2	1.00	0.25
Mode 2′	1.40	0.21
Mode 3	3.65	0.25

Table 3: Aerosol particle size distribution as used in this work. All size distributions are log-normal.

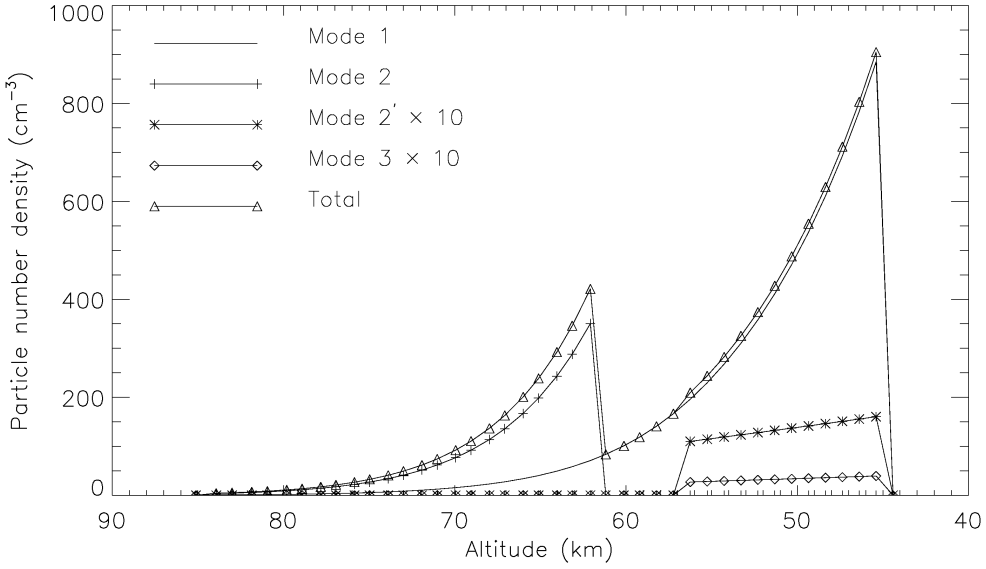

Figure 4: Vertical distributions of the four cloud particle size modes used in this work.

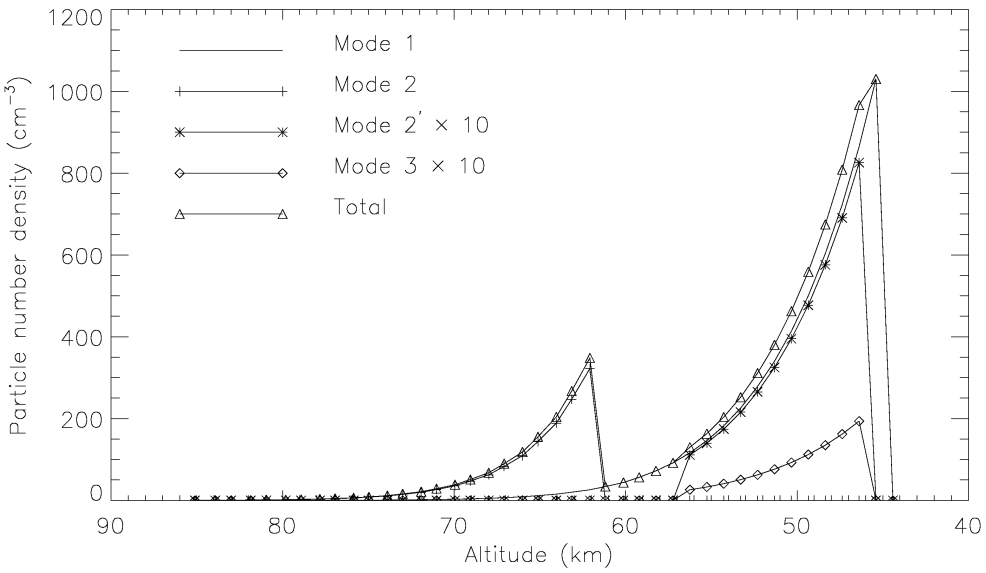

Figure 5: Vertical distributions of the four cloud particle size modes as given in Pollack et al. (1993).

4 Cloud Microphysics

4.1 Cloud formation on the Earth

Cloud formation on the Earth can be used as a useful illustration of the sort of physical processes that may cause the formation of cloud on Venus. Cloud formation on the Earth relies on convective processes. Parcels of moist air rise due to convection in the atmosphere, and when the temperature of such a parcel falls below the dew point temperature it reaches saturation with respect to water (Rogers & Yau 1989). Once saturation is achieved, water vapour can condense out and form cloud droplets, provided there are sufficient cloud condensation nuclei.

Adiabatic expansion and contraction of dry air can be described using the first law of thermodynamics. In differential form, this can be stated as

$$\mathrm{d}q = c_p \mathrm{d}T - \alpha \mathrm{d}p, \tag{6}$$

where $\mathrm{d}q$ is the change in heat per unit mass, c_p is the specific heat capacity for constant pressure, T is temperature, $\mathrm{d}p$ is change in pressure and α is the volume per unit mass. For an adiabatic process, $\mathrm{d}q$ is zero. If, however, the air is not dry but moist, we have to take into account the effect of water

on these processes. When water is in the vapour phase, we can treat it as an ideal gas (Rogers & Yau 1989), allowing us to use the equation of state for an ideal gas to define the vapour pressure, e:

$$e = \rho_v R_v T, \tag{7}$$

where ρ_v is the density of the water vapour and R_v is the individual gas constant for water vapour.

The evaporation of water requires heat. The latent heat of vaporisation is the heat energy required to convert a unit mass of water into water vapour, assuming no change in the pressure or temperature. The latent heat L is given by

$$L = \int_{q_1}^{q_2} \mathrm{d}q = \Delta u + e_s \Delta\alpha, \tag{8}$$

where e_s is the vapour pressure at which the air is saturated with respect to water vapour and Δu is the change in internal energy between the two states. Given that we have assumed T is constant, we can also write this as

$$L = T \int_{q_1}^{q_2} \frac{\mathrm{d}q}{T} = T\Delta s, \tag{9}$$

where s is the entropy per unit mass. Equating (8) and (9) allows us to find a conserved thermodynamic quantity that we will call the Gibbs free energy G:

$$G = u + e_s\alpha - Ts. \tag{10}$$

Conservation of the differential $\mathrm{d}G$ leads to the Clausius-Clapeyron equation:

$$\frac{\mathrm{d}e_s}{\mathrm{d}T} = \frac{\Delta s}{\Delta\alpha} = \frac{L}{T\Delta\alpha}. \tag{11}$$

The saturation vapour pressure defines the point at which condensation of water vapour is energetically favourable, and the Clausius-Clapeyron equation gives the temperature dependence of this quantity. Thus, the predominant mechanism on the Earth lading to supersaturations is cooling.

However, this rather simplistic model does not entirely describe the full requirement for cloud formation. The Clausius-Clapeyron equation does not take into account the free energy barrier for condensation of water into small droplets (Rogers & Yau 1989), so in fact condensation into droplet form might not be expected to occur until large supersaturations of water vapour are reached. In reality, we do observe the formation of cloud particles for small supersaturations because the air contains micron and sub-micron particles

that act as a source of cloud condensation nuclei (CCN), facilitating droplet formation without the need for large supersaturations.

The saturation vapour pressure for a spherical droplet is dependent on the radius of curvature, and is given below by the Kelvin equation:

$$e_s(r) = e_s(\infty)\exp\left(\frac{2\sigma}{R_v\rho_l T r}\right), \tag{12}$$

where r is the radius of curvature of the droplet, σ is the surface tension and ρ_l is the density of the liquid. A droplet must therefore achieve a critical size if it is to be stable, as the vapour pressure must equal this saturation vapour pressure for the rates of evaporation and condensation to be balanced (Rogers & Yau 1989). Particles greater than this size are said to be 'activated' and it is favourable for them to grow by condensation. Formation of droplets of the critical size can occur by a variety of processes, listed by Houze, Jr. (1993). The growth of a drop of pure water by condensation alone is homogeneous nucleation, whereas the growth of a droplet around an aerosol particle is heterogeneous nucleation. Heterogeneous nucleation is by far the more important of these two processes on Earth. Cloud droplets can also grow when smaller droplets collide and coalesce, which is best modelled as a discrete process called stochastic collection. This model results in a more realistic size distribution than an assumption of continuous growth as it takes into account the possibility that two drops of the same initial size may not attain the same size after a time Δt, as they may experience different numbers of collisions.

4.2 Cloud Microphysics on Venus

The mechanisms for cloud formation on Venus are poorly understood by comparison with those on Earth, but the theory above can still be applied. A very simple cloud formation process for Venus is outlined in Figure 6.

A multi-modal distribution as observed in the Venusian cloud favours a stochastic collection model for the initial growth and activation of cloud droplets. Knollenberg & Hunten (1980) suggest that the smallest mode 1 particles have not yet reached the critical radius and are not yet activated, so remain small as they can only grow by coalescence, whereas mode 2 particles have achieved this critical radius and so can grow to larger sizes more easily, explaining the marked difference in average size between these two modes. Cloud condensation nuclei are believed to be an important part of this process - indeed, Knollenberg & Hunten (1980) suggest that the smallest mode one particles detected by the Pioneer Venus LCPS in the lower cloud may be just bare CCN, with little sulphuric acid content. Imamura & Hashimoto (2002)

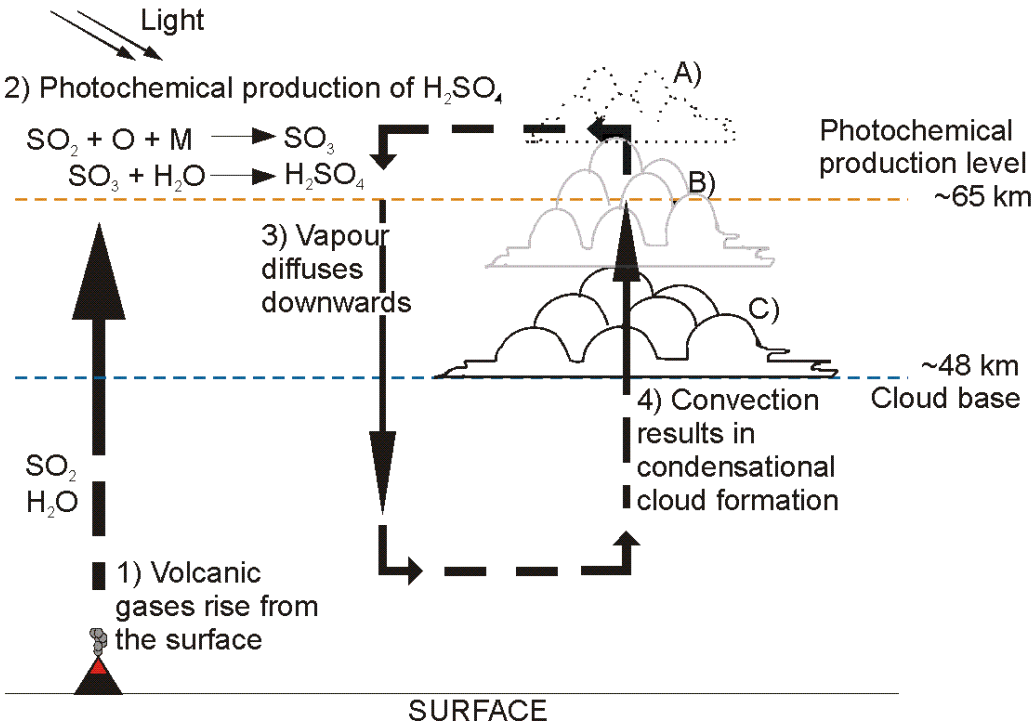

Figure 6: A simple schematic of how sulphuric acid clouds may form on Venus. A) marks the upper haze, B) is the upper cloud composed of mode 1, mode 2 and UV absorber particles, and C) is the lower cloud made mostly of mode 2' and mode 3 particles, as described by Crisp (1986) and Pollack et al. (1993).

assume the CCN to be made of elemental sulphur, with a single radius of 0.17 μm, based on the LCPS measurements discussed by Knollenberg & Hunten (1980).

The formation mechanism for mode 3 particles is less certain. Knollenberg & Hunten (1980) suggest that these particles may be crystalline. Other models treat all modes as composed of concentrated sulphuric acid (see Section 3.1). The model of Imamura & Hashimoto (2002) results in mode 3-sized particles being produced by condensation of sulphuric acid as a result of vigorous diffusion in the region of the lower clouds.

Bullock (1997) in his thesis on the stability of the Venusian climate utilised a simple chemical and microphysical model for cloud feedback processes. This model took into account the photochemical formation of H_2SO_4 aerosols and the subsequent diffusion/convection/condensation processes as shown in Figure 6. A relationship between particle size and number den-

sity was obtained by setting equal the Stokes drift timescale of the particles and the Brownian coagulation timescale of aerosols. The aerosol vapour was assumed to be destroyed at a temperature of 432 K, which occurs around 40 km altitude. The resulting particles were then binned according to size and composition, and this distribution was used in the radiative transfer calculations.

McGouldrick & Toon (2007) and McGouldrick & Toon (2008) also implement a microphysical cloud model to investigate the mesoscale spatial evolution of the Venusian condensational clouds. They use the Community Aerosol and Radiation Model for Atmospheres (CARMA) to investigate the evolution of 'holes' in the cloud and the effect of convection cells and gravity waves. They use the values of Knollenberg & Hunten (1980) at 40 km as the CCN input distribution for their microphysical model.

The results of these different microphysical models suggest that simple microphysical parameterisations can be useful in modelling the behaviour over time of the Venusian cloud. The work of Knollenberg & Hunten (1980) provides a good physical basis for a multi-modal cloud as observed on Venus. In summary, it seems likely that the size distribution of the Venusian cloud is achieved through stochastic collection followed by preferential condensational growth of larger particles, although this does not rule out the possibility that the mode 3 particles may have an entirely different origin.

5 Branch Plot Method and Results

5.1 Method

The branch plot method uses a comparison between the radiances at two different wavelengths to study the variation of a parameter. This can be a parameter of the cloud that affects the spectral behaviour of infrared absorption or scattering by the cloud particles, or it could be the abundance of a gas that has an absorption band at one of the two wavelengths chosen. Synthetic spectra are created using *NEMESIS* for different amounts of mode $2'$. Mode $2'$ abundance varies along each branch, and different branches are produced by changing other model input parameters, such as mode 3 abundance. These branch plots define a parameter space that may depend on one or more of the varying input quantities. If the parameter space depends on only one variable, the position of a data point from a real spectrum on the branch plot allows the variable to be fixed for that data point. Once this variable is fixed, branch plots that are sensitive to this variable and one other can be used to fix a second variable, and so on.

The variables of interest in this work are mainly related to the cloud. They are the concentration of the acid in the cloud particles, the abudance of mode 3 particles and the altitude of the cloud base. In the spectral window regions at 1.74 µm and between 2.15 and 2.6 µm there are absorption bands due to CO, H_2O and OCS. The OCS absorption has little effect on the wavelengths used in this study, so has not been discussed here. The spectral sensitivity to these parameters is shown in Figure 7.

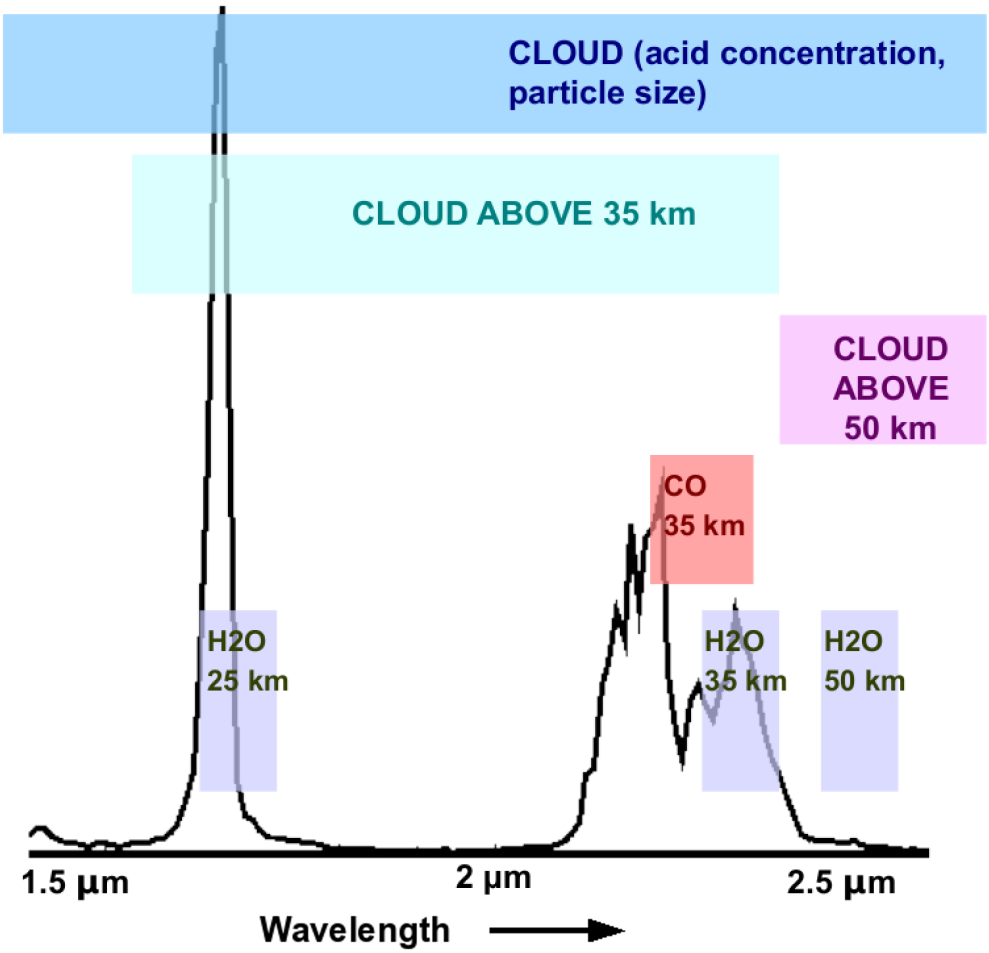

Figure 7: Sensitivity to the acid concentration, mode 3 abundance, base altitude and CO and H_2O between 1.6 and 2.6 µm.

Branch plots have been generated for combinations of radiances at 1.74, 2.2, 2.3, 2.32, 2.4 and 2.53 microns, to investigate variation in acid concentration, fractional abundance of mode 3 particles, cloud base altitude, CO abundance at 35 km and H_2O abundance at 35 km. A branch plot for 2.2

μm radiance against 1.74 μm radiance is sensitive only to the concentration of the acid in the clouds. Figure 8 shows radiances at these wavelengths for a series of models with acid concentrations of 85% and 96%, fractional mode 3 abundances of 1, 1.5 and 2, and cloud base altitudes of 44, 48 and 52 km. It can be seen that the model branches with different mode 3 fractional abundances and cloud base altitudes lie on top of each other, so the only mode of variability in this parameter space is the acid concentration.

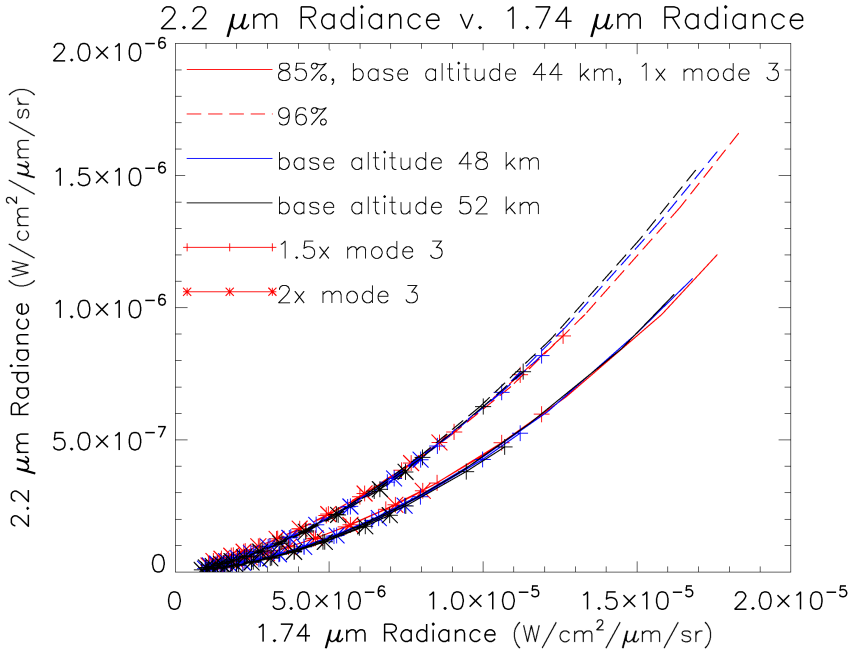

Figure 8: Model branches for 2.2 against 1.74 microns. Dashed and continuous lines represent different acid concentrations, different colours different base altitudes, and different symbols different amounts of mode 3. The two distinct branches are formed by varying the acid concentration.

Four other parameters remain to be constrained. After correction for acid concentration, the ratio between radiances at 2.3 and 1.74 microns may be used to determine the relative abundance of large mode 3 particles, which when compared with the abundance of mode 2′ particles is an indicator of average particle size (Figure 8). The base altitude can be determined using the ratio of radiances at 2.53 and 2.4 microns, after correcting for acid concentration and CO abundance (Figure 10. The gaseous abundances can be calculated using the ratios of 2.32 to 2.3 micron radiance (CO, Figure 12) and 2.4 to 2.3 micron radiance (H_2O, Figure 12).

Each branch in the branch plots is fitted using a linear, second-order polynomial or third-order polynomial trendline. The coefficients of these fits can then be linearly related to the variable of interest, and this relationship can be used either to calculate a value for that variable or introduce a correction if the value is already known. The correlation coefficients for all fits are good (>0.99) but not perfect, and this imperfection is a source of error. The error can be quantified by applying the method to model data points with known input values, and comparing the results with the correct values. The errors calculated are shown in Figure 14 as a function of 1.74 μm radiance.

5.2 Data Processing

The data used have been spatially coadded in boxes of 20 × 20 pixels, shifted every 10 pixels to ensure Nyquist sampling. This reduces a 256 × 256 pixel image to a 25 × 25 pixel image. Single radiances for 1.74, 2.2, 2.29, 2.32, and 2.4 microns have been extracted for each coadded spectrum. The 2.53 μm radiance used has been smoothed using a triangular filter in order to remove the odd-even effect, which is a discrepancy in the response of odd and even spectels in the spectral dimension of VIRTIS-M and is more prounounced at low radiances. This smoothing calculates the 2.53 μm radiance as $I'_{2.53} = 0.25 \times I_{2.52} + 0.5 \times I_{2.53} + 0.25 \times I_{2.54}$.

The VIRTIS viewing geometry results in the planet being observed at a range of emission angles. The emission angle of the radiation coming from the planet affects the radiance measured, as the atmospheric path travelled is greater for higher emission angles. This effect is known as limb darkening. A correction for this effect has been applied to each of the radiances used in this work. The correction was obtained by creating model spectra for different input emission angles, and deriving a relationship between emission angle and radiance.

5.3 Low- to Mid-Latitude Results

Spatial variation in results for observation 0319_00[1] are shown in Figure 13. It can be seen that there is some correlation between fractional cloud amount as indicated by the 1.74 μm radiance, acid concentration, cloud base altitude and fractional abundance of mode 3 particles. Variations in abundances of CO and H_2O, on the other hand, do not appear to be correlated to the cloud parameters. However, if the results for all observations in Table 4 are binned

[1] Observation numbers consist of a 4-digit orbit number followed by a 2-digit observation number, starting from 00. For example, observation 0321_02 was the third observation recorded in orbit 0321.

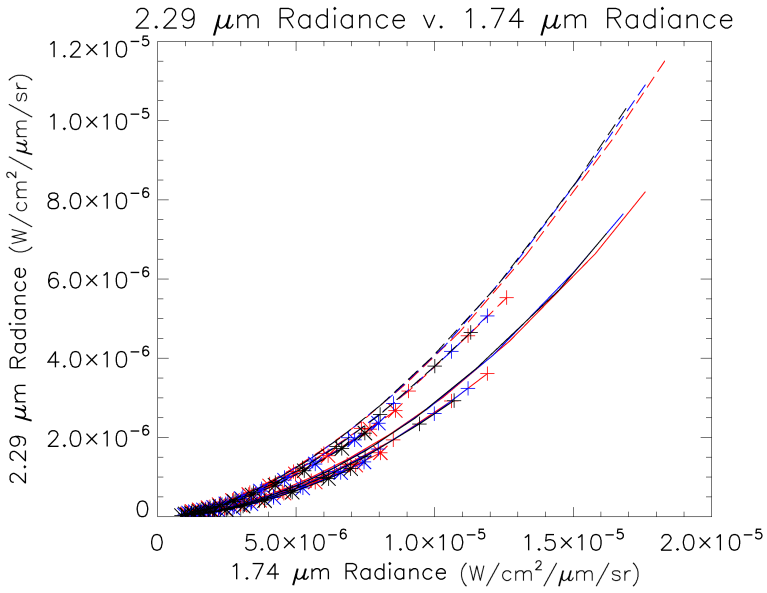

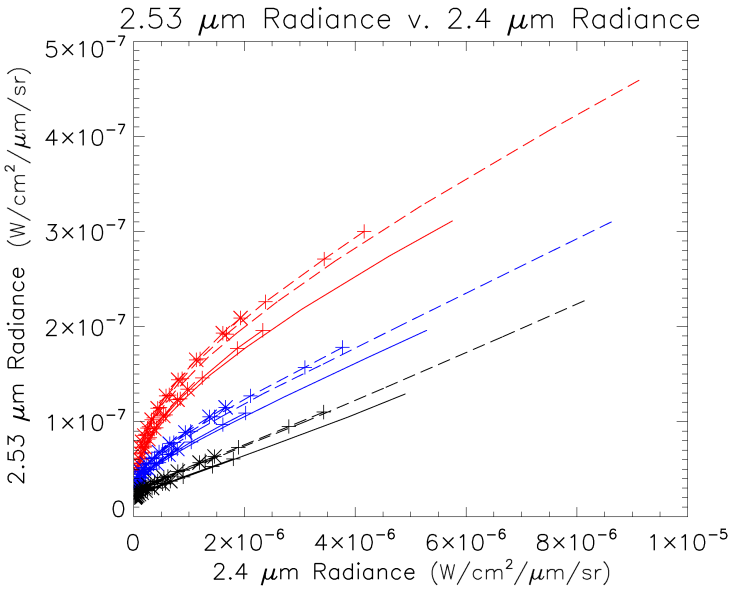

Figure 9: Model branches for 2.3 against 1.74 μm. Symbols, line styles and colours are as in Figure 8. The two distinct branches formed by varying the acid concentration are each split into three by varying the fractional mode 3 abundance.

Figure 10: Model branches for 2.53 against 2.4 μm. Symbols, line styles and colours are as in Figure 8. The three distinct branches are formed by varying the base altitude.

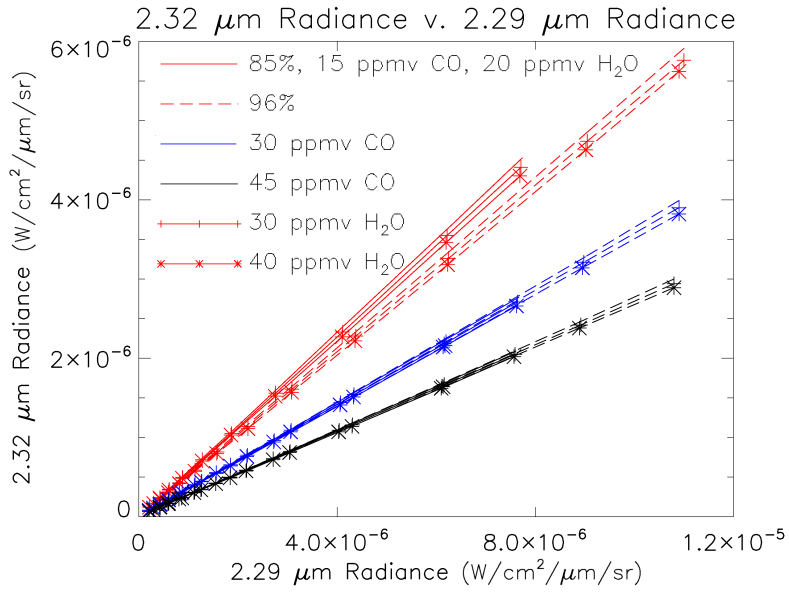

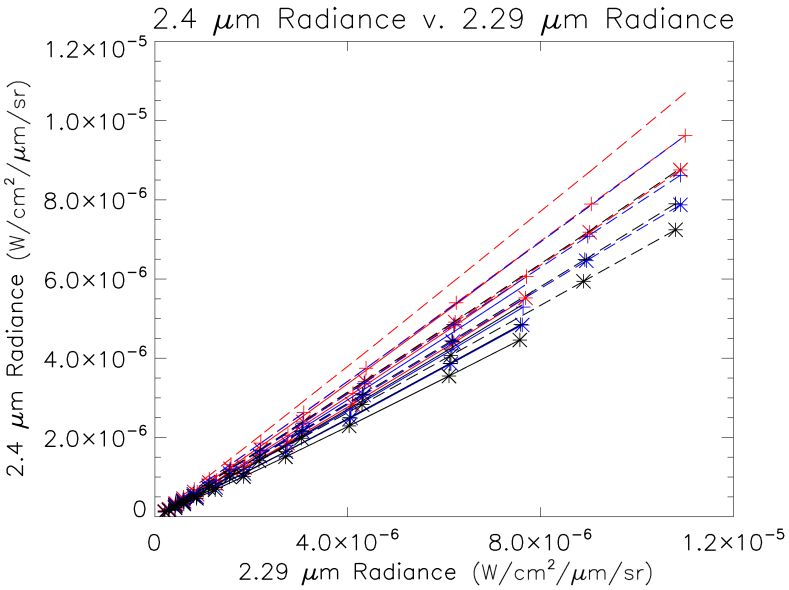

Figure 11: Model branches for 2.32 against 2.3 μm. Dashed and continuous lines represent different acid concentrations, different colours different CO abundances, and different symbols different H_2O abundances. The three branches are formed by varying the CO abundance.

Figure 12: Model branches for 2.4 against 2.3 μm. Symbols, line styles and colours are as in Figure 11. Branches are formed by varying CO and H_2O abundances.

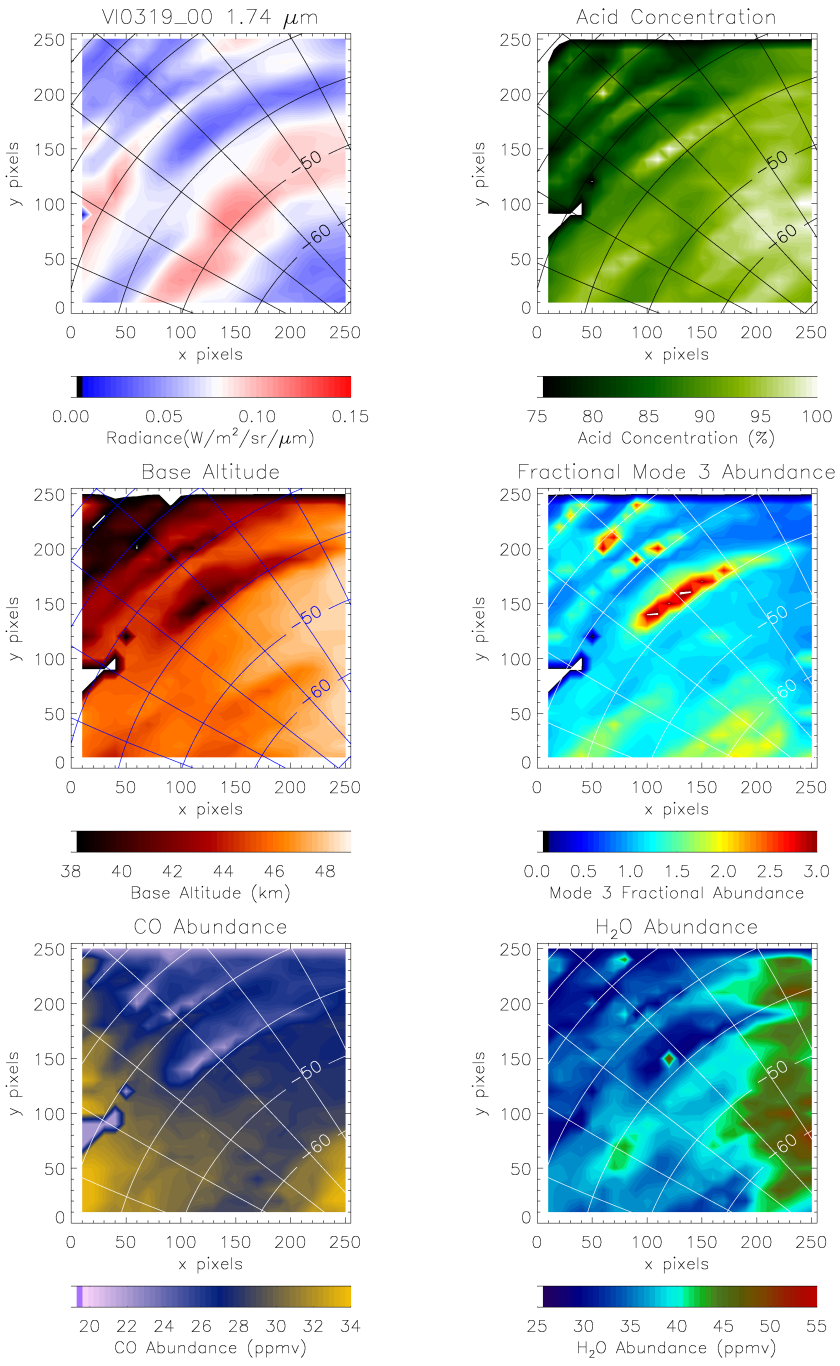

Figure 13: Results for the observation 0319_00. There is some spatial correlation between fractional cloud amount, acid concentration and mode 3 fractional abundance, and some negative correlation between base altitude and fractional cloud amount.

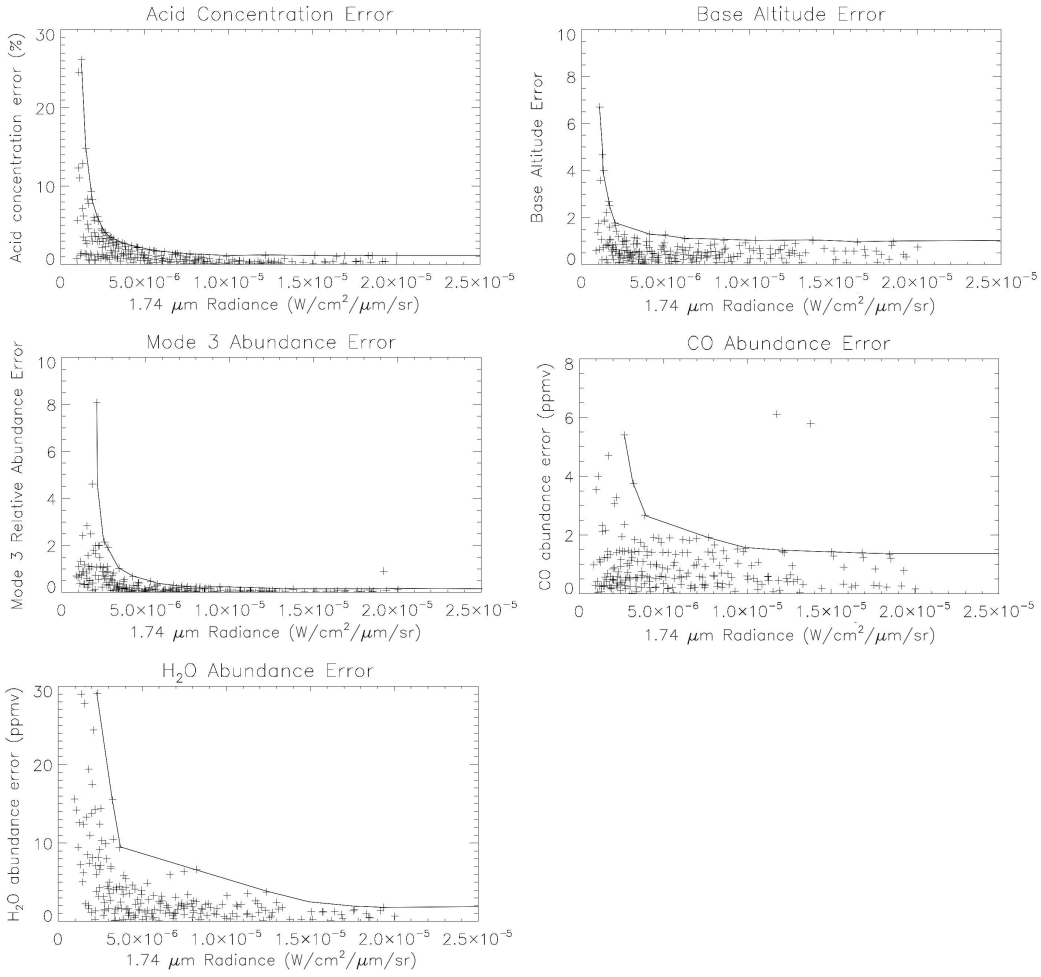

Figure 14: Errors for each variable, given by the modulus of the difference between actual and computed values for model spectra. The line represents the maximum values, excepting outliers, for each radiance and these were used as the final error values.

in 1.74 micron radiance and averaged, the water vapour abundance is seen to increase slightly with increasing radiance (Figure 19). Acid concentration is clearly shown to increase with decreasing radiance (Figure 15), as does the relative abundance of mode 3 particles (Figure 17), whilst the base altitude increases with increasing radiance (Figure 16). The CO abundance still has no apparent correlation with cloud features or 1.74 μm brightness (Figure 18) It can seen in Figures 8—12 that for low radiance models the spread between the model branches generated for different input parameters decreases. Because of this effect results obtained for low radiance points using this method are potentially unreliable, so in Figures 15—19 only data points with 1.74 μm radiances above 0.05 W/m^2/μm/sr are included.

Observation	Min. Latitude	Max. Latitude
0319_00	-71	15
0319_01	-41	17
0320_01	-66	-6
0320_02	-48	0
0321_01	-40	18
0321_02	-32	24
0334_02	-48	0
0359_02	-54	-2
0373_02	-56	0
0382_02	-65	-24

Table 4: Low- to mid-latitude observations, with latitude ranges, used in Figures 15—19.

5.4 Polar Results

The polar cloud on Venus is even less well-understood than the low-latitude cloud. It is clear from Venus Express results that there is significant variation in the dynamics and the cloud properties from $\sim -60°$ latitude to the pole, but few conclusive results have been obtained relating to the changing cloud properties. It is however apparent that model spectra that match spectra from low- to mid-latitude regions do not provide a good fit to polar spectra. Carlson et al. (1993) and Wilson et al. (2008) have used the ratio of 1.74 to 2.3 μm as a proxy for cloud particle size, as in this work, and both studies found an increase in average particle size towards the pole, providing some explanation for the poorness of fit. Erard et al. (2009) also suggested this may be the case, as one orthogonal mode of variability in their independent component anaylsis was relative variation between the 1.74 and 2.3 μm

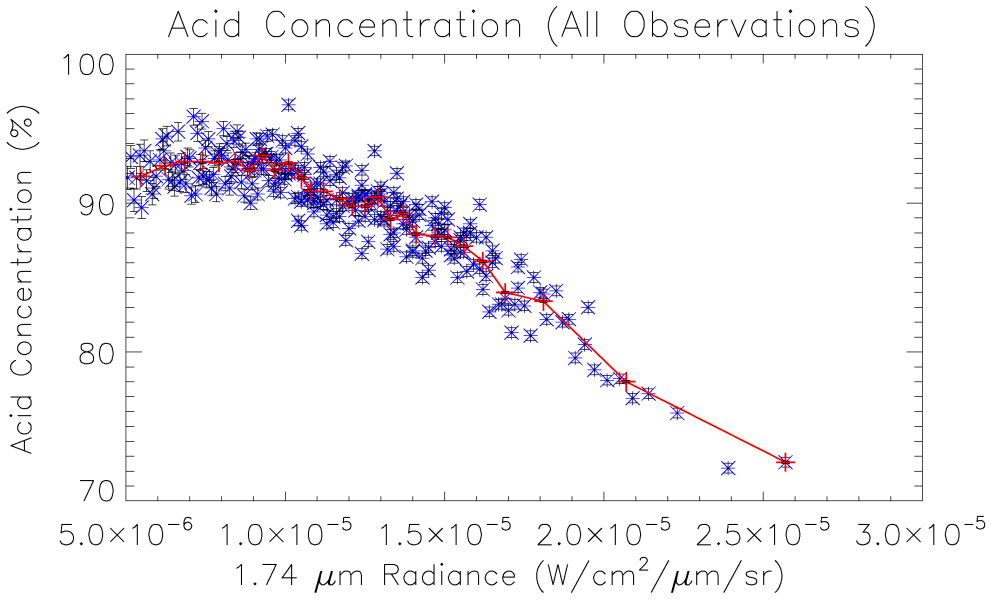

Figure 15: Inverse correlation between acid concentration and 1.74 μm radiance. The blue points are data from the observations listed in Table 4, averaged in radiance in bins of 15 points. The red points are averaged again in bins of 10 points.

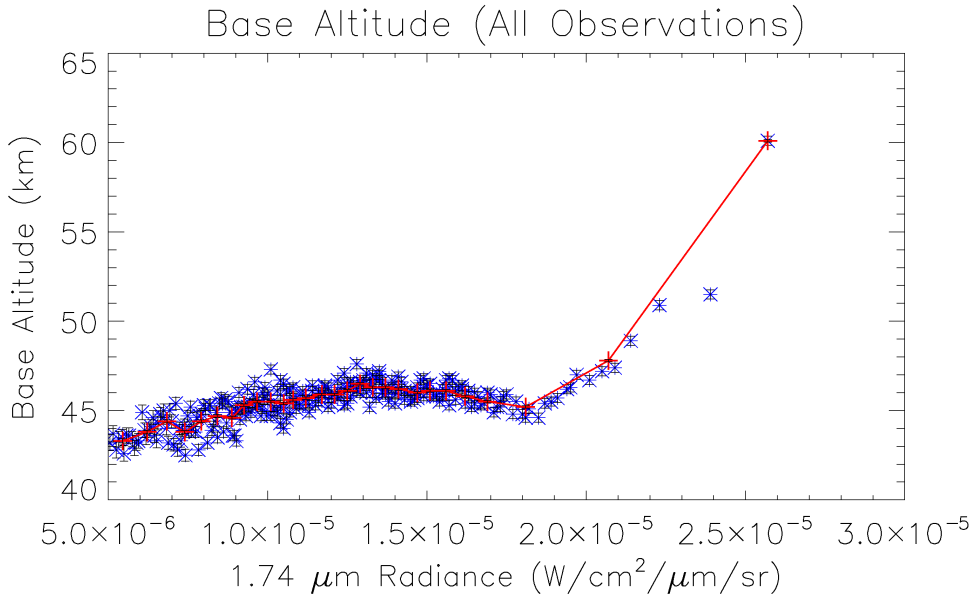

Figure 16: Positive correlation between base altitude and 1.74 μm radiance. Colours are as in Figure 15.

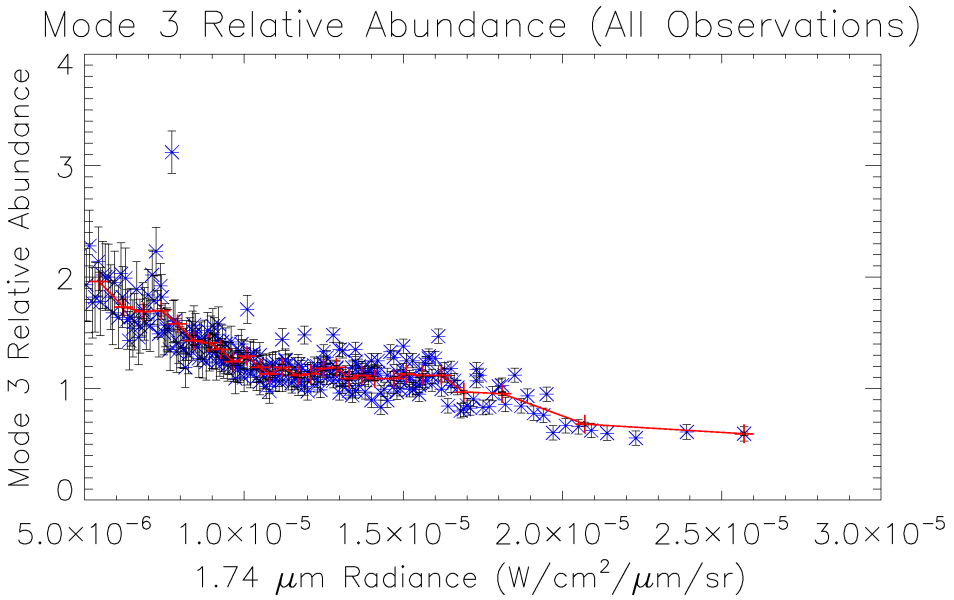

Figure 17: Inverse correlation between mode 3 relative abundance and 1.74 μm radiance. Colours are as in Figure 15.

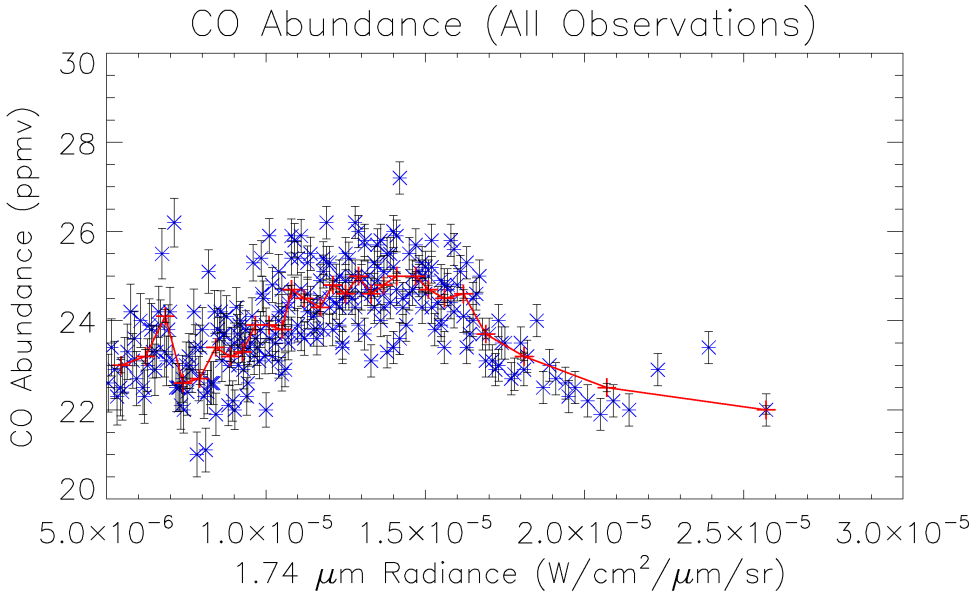

Figure 18: Little or no correlation between carbon monoxide abundance and 1.74 μm radiance. Colours are as in Figure 15.

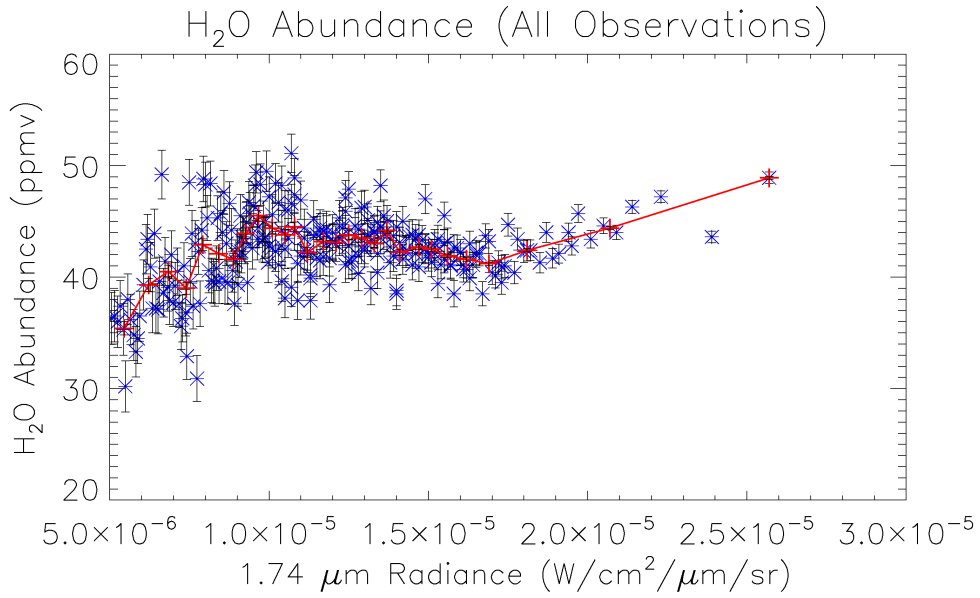

Figure 19: Slight positive correlation between water vapour abundance and 1.74 μm radiance. Colours are as in Figure 15.

peaks, and maps of this component showed banded structures in concentric rings around the south pole. However, none of these investigations took into account potential variation in cloud acid concentration, which is shown to also affect the radiance ratio between these two wavelengths. The analysis in this work takes such variation into account, and therefore has the potential to come up with a robust a priori cloud parameterisation for the polar regions.

Observation	Min. Latitude	Max. Latitude
0320_00	-86	-25
0321_00	-71	15
0334_00	-84	-26
0344_00	-83	-28
0382_00	-89	-26

Table 5: Polar observations, with latitude ranges, used in Figure 20.

Five observations with good coverage of the south pole were chosen, and these are listed in Table 5. Points with a signal-to-noise ratio lower than 100 were excluded from the analysis. The method used was as above, except that a correction was added for each radiance ratio based on the assumed change in temperature structure at 60° latitude. The correction was obtained by

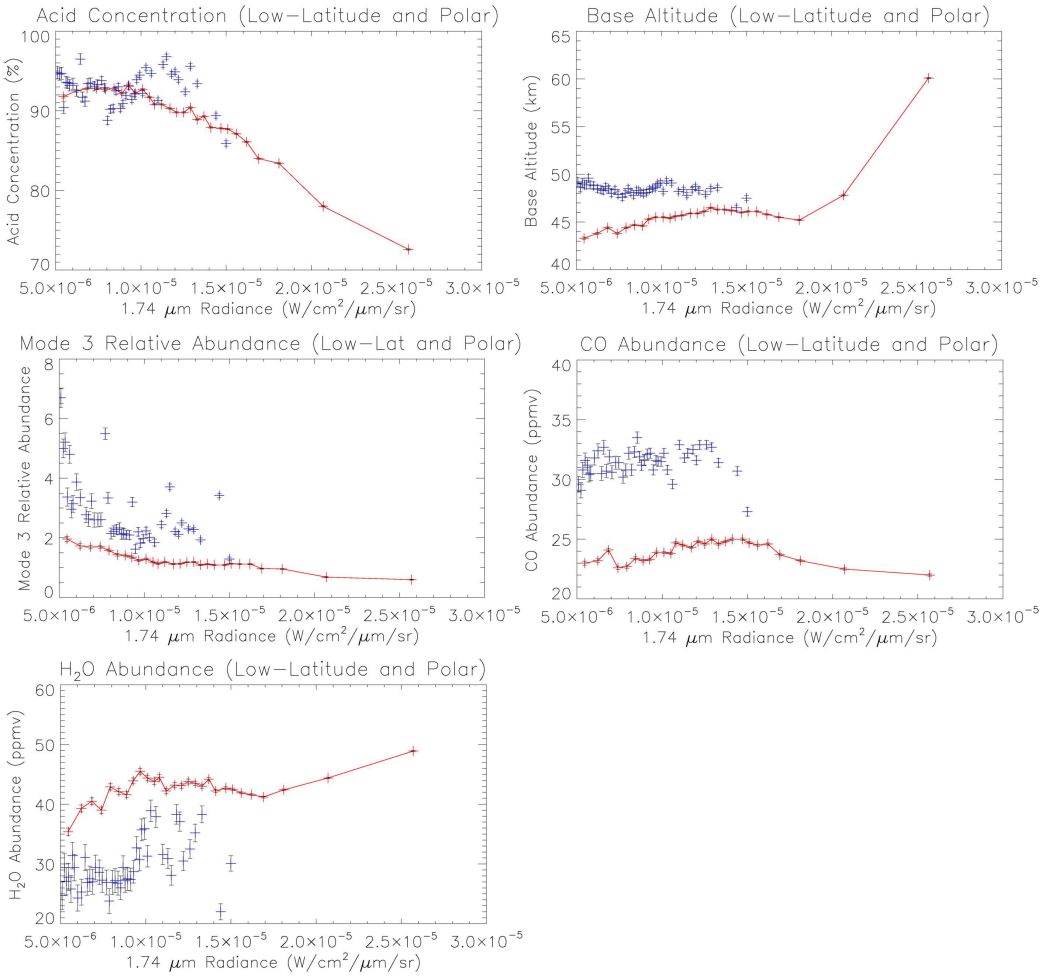

Figure 20: Scatter plots for polar observations, averaged in 1.74 μm radiance in bins of 15 points, compared with doubly-coadded plots from Figures 15—19. Polar data are in blue.

generating model spectra for the a priori case and for a 60° latitude temperature profile from the Venus International Reference Atmosphere (Kliore et al. 1986). Branches were then plotted for these two cases and a correction factor for each plot obtained. This is of course a somewhat crude method, since the temperature profile varies with latitude, but the currently available temperature data preclude a more detailed investigation.

Scatter plots for these data are shown in Figure 20, alongside the low- to mid-latitude results. It can be seen that the trends are somewhat different in the polar region. The variation of acid concentration with 1.74 μm radiance is similar across the planet, but the base altitude variation is barely present and values are higher for the same radiances than those at lower latitudes. The mode 3 abundance values show a similar decreasing trend with radiance, but are approximately twice the magnitude in the polar region. This fits well with the observations of Carlson et al. (1993) and Wilson et al. (2008). The CO abundance is approximately constant with radiance, but the values average around 32 ppmv instead of 24 ppmv. These results are also consistent with previous measurements (Tsang et al. 2008b, Tsang et al. 2009). There is no obvious trend with radiance in the water vapour abundance measurements, but the measured abundances are lower, falling in the range 20—40 ppmv instead of 30—50 ppmv. As might be expected, these results suggest the atmosphere in the polar region is significantly different from that at latitudes above -60°. Therefore, looking at the behaviour of these quantities as a function of latitude would provide further insight into dynamical and compositional changes with latitude in the Venusian atmosphere.

5.5 Latitudinal Variation

Figure 21 shows scatter plots produced in the same way as Figures 15—19, except with points are binned in latitude instead of radiance. Some interesting trends become apparent: there is a small increase in the acid concentration and base altitude towards the poles, and the expected increase in CO from Tsang et al. (2008b) and Tsang et al. (2009) is observed. There is also an increase in the mode 3 relative abundance, although the scatter in the polar region is large. The most interesting result is the strong decrease in water vapour abundance towards the poles, which has not been observed before – a previous study of the latitudinal variation of water vapour abundance by Marcq et al. (2008) did not examine points beyond -60° latitude. The lack of obvious trend in water vapour abundance between the equator and -60° is consistent with the results of Marcq et al. (2008), although the absolute values in this work are higher by about 10 ppmv. This is probably due to the 75% acid concentration used in the model of Marcq et al. (2008), as described

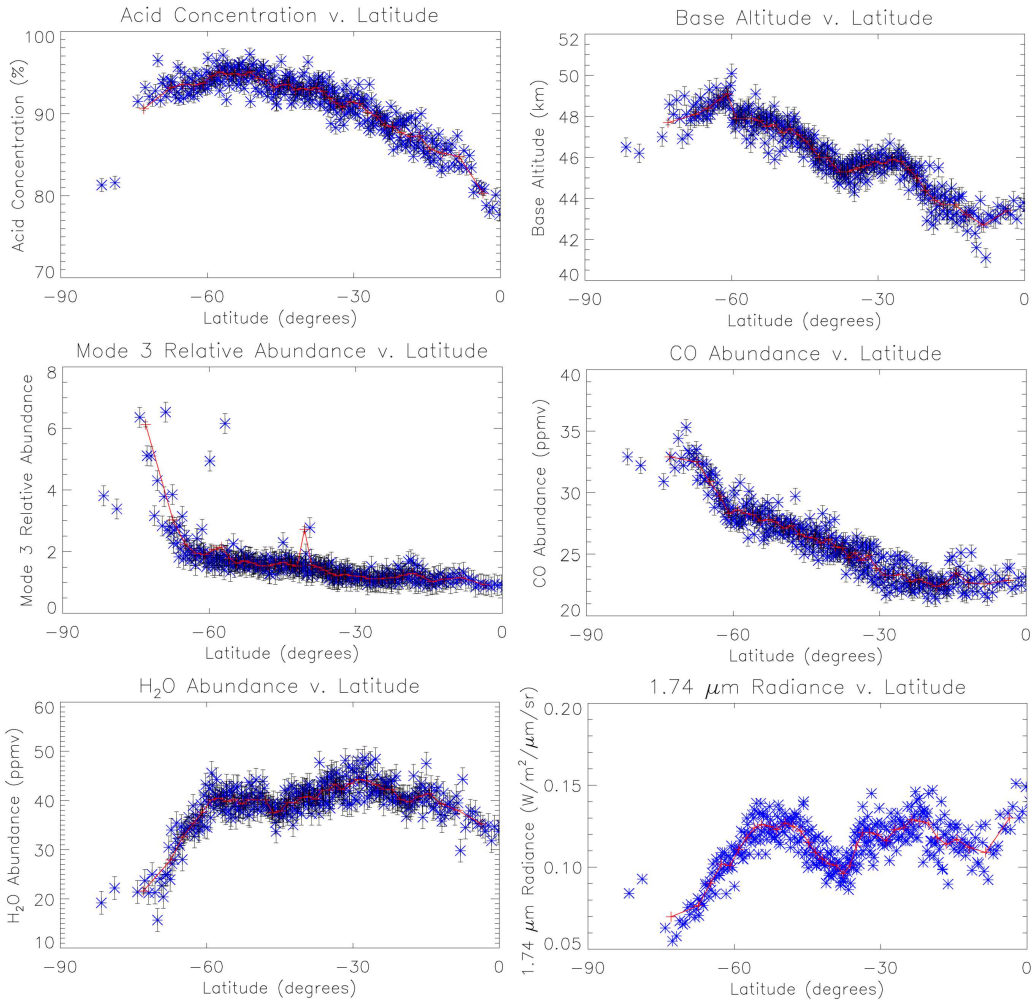

Figure 21: Scatter plots showing behaviour of all variables as a function of latitude, averaged in latitude in the same was as the radiance average in Figures 15—19. All points with 1.74 μm radiances below 0.05 W/m^2/μm/sr were disregarded.

in Marcq et al. (2006). As explained in Tsang et al. (2010, in preparation), a water vapour retrieval in the 2.3 μm window using an assumed cloud model with 96 wt % H_2SO_4 yields a higher retrieved abundance of water vapour than the same retrieval with an assumed cloud acid concentration of 75 wt %. The magnitude of this difference is approximately 20 ppmv. The difference between the average result of Marcq et al. (2008) and the low- to mid-latitude result in this work is somewhat less, with the values for this work between 38 and 48 ppmv and the Marcq et al. values between 28 and 34 ppmv. However,

the results of Marcq et al. are inherently biased towards higher radiances due to the low signal-to-noise of VIRTIS-H, the instrument used in their work, and we find that the abundance of water vapour is generally higher in regions of higher radiance, along with Tsang et al. (2010) and Tsang et al. (2010, in preparation). This would suggest that an average value obtained by Marcq et al. is likely to be higher than a similar value obtained using VIRTIS-M data with the same underlying model assumptions.

6 Discussion and Initial Conclusions

6.1 Spatial Variation

Our work suggests that the three free cloud parameters we have calculated are correlated with the 1.74 μm radiance, which is a proxy for the total amount or optical thickness of the cloud. We draw three conclusions about the behaviour of the Venusian cloud:

1. The concentration of sulphuric acid in the cloud particles increases as the number of cloud particles increases

2. The altitude of the cloud base is lowered as the number of cloud particles increases

3. The relative abundance of mode 3 particles increases as the number of cloud particles increases.

There is also a slight anti-correlation between the abundance of water vapour and the number of cloud particles. This phenomenon has already been discussed extensively in Tsang et al. (2010) and Tsang et al. (2010, in preparation), and will be dealt with briefly here in Section 6.3.

In order for clouds to form, the atmosphere must be supersaturated with respect to the cloud-forming component. Higher supersaturations result in cloud formation becoming more energetically favourable. James et al. (1997) found that halving the abundance of sulphuric acid vapour below the cloud in their microphysical model raised the altitude of the cloud base by approximately 2 km and thereby reduced the total number of particles in the cloud – as would be expected, a lower abundance of sulphuric acid vapour results in less cloud being formed. This work indicates that the cloud base altitude on Venus does increase in regions where less cloud is formed, which is consistent with the results of this model.

It is also conceivable that as the abundance of sulphuric acid vapour increases, cloud particles with a higher acid concentration become more energetically favourable. The mechanism determining the concentration of the sulphuric acid in the Venus clouds is poorly understood, but it must depend on the relative availability of sulphuric acid vapour and water vapour.

The mode 3 relative abundance increases as the total amount of cloud increases, but this is of course not unexpected - it simply suggests that there is a proportional increase in the abundances of mode 2′ and mode 3 particles as the total amount of cloud increases. If we use the known amount of mode 3, acid concentration and 1.74 μm radiance we can determine a relative abundance for mode 2′ as well as for mode 3. The ratio of mode 3 abundance to mode 2′ abundance increases with increasing radiance, initially slowly but increasingly rapidly for higher radiances (Figure 22). This is perhaps initially counter-intuitive, however, it is likely that smaller particles will more easily evaporate when conditions are less favourable for cloud formation, and will also form more rapidly in favourable conditions than larger particles. Fluctuation in the relative abundance of mode 3 particles is therefore likely to be less extreme than for mode 2′.

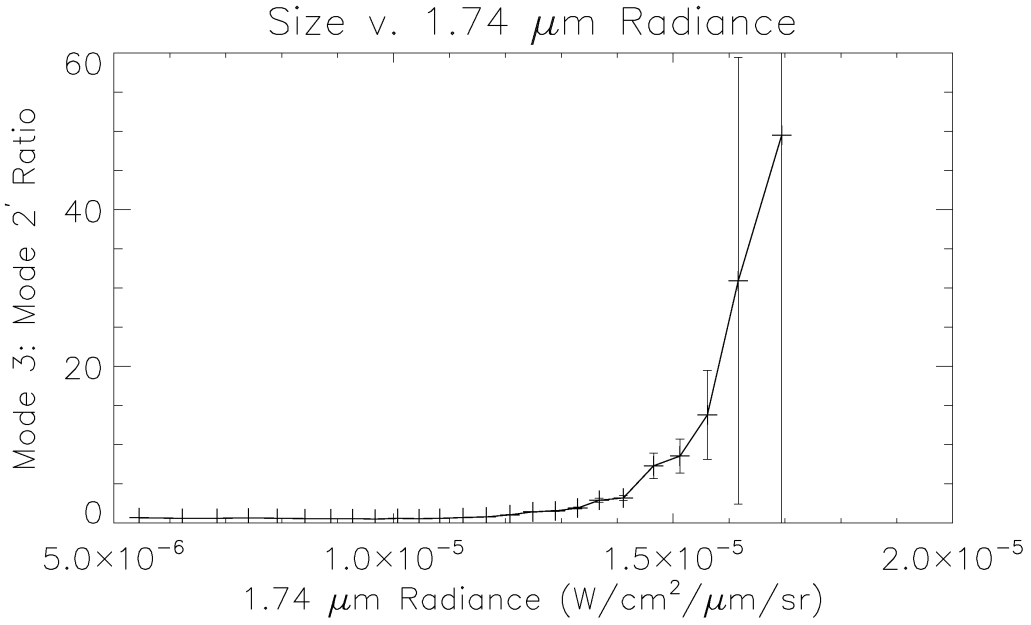

Figure 22: Ratio of mode 3 to mode 2′ relative abundance against radiance, averaged twice in radiance as in Figure 15.

6.2 Latitudinal Variation

There are indications of small but statistically significant latitudinal variation in cloud parameters in the results presented in Section 5. These are summarised as follows (see schematic in Figure 24):

1. The concentration of sulphuric acid in the cloud particles increases slightly towards the polar region, with a peak at around -60° followed by a decrease closer to the south pole.

2. The altitude of the cloud base increases towards the pole, with some small fluctuations that are correlated with the latitudinal radiance fluctuation (Figure 21)

3. The relative abundance of mode 3 particles increases towards the pole, more sharply at latitudes beyond -70° (Fgure 23).

It has been suggested by several authors that the downwelling branch of a Venusian Hadley cell may be present at -60° latitude (Titov et al. 2008, Tsang et al. 2008b). The behaviour of the acid concentration as a function of latitude may reflect this also, as there is a peak at -60°. This may be due to downwelling drawing down drier air and reducing the amount of water vapour available in the cloud-forming region, thus making the formation of more acidic cloud more favourable.

The increase in the altitude of the cloud base towards the pole is less straightforward to explain. This increase is associated with lower cloud opacities where there is correlation with radiance, but this is unlikely to be the case here as the cloud opacity is generally higher in the polar region. This may also be due to downwelling resulting in drier air in the cloud layer, which may raise the altitude at which condensation is favourable, since this altitude is dependent on the abundances of water vapour and sulphuric acid.

Wilson et al. (2008) attempted to explain the increase in particle size towards the poles, which we also observe. One explanation offered was that the downwelling at the poles removes the more volatile smaller particles from the cloud and results in their evaporation. This is a similar explanation to the one we offer for the increase in particle size in regions of thin cloud: however, this is inconsistent with the presence of optically thick cloud in the polar region. An alternative suggestion offered by Wilson et al. (2008) is that the composition of the cloud particles changes towards the poles. The precise chemical nature of the mode 3 particles has long been questioned, with several suggestions put forward by various authors. Apart from the hypotheses by Esposito et al. (1983) and Cimino (1982) outlined in Section 3, Knollenberg & Hunten (1980) suggest that these large particles may be crystalline, and

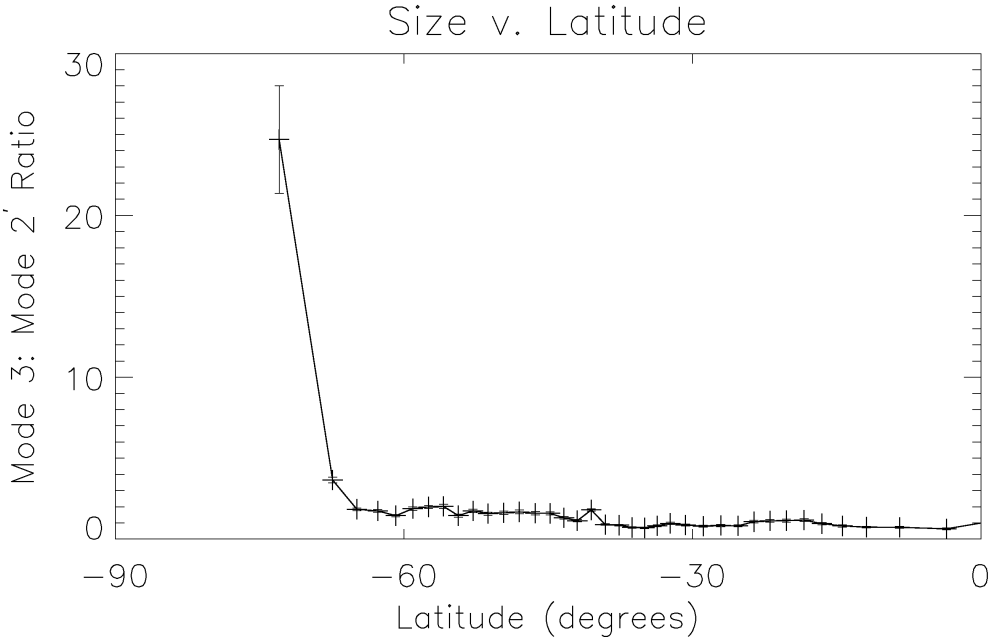

Figure 23: Ratio of mode 3 to mode 2′ relative abundance against latitude, averaged twice in latitude as in Figure 21.

several alternative chemical compounds have been proposed by Krasnopolsky (1989), including aluminium chloride and hydrogen phosphate.

6.3 Gaseous Variation

This work has, for completeness, determined the abundances of CO and H_2O at 35 km as functions of radiance and latitude, after taking into account variation in cloud parameters. The findings are summarised below:

1. The abundance of CO is approximately constant with radiance, with values between 22 and 26 ppmv. There is however a significant increase in abundance with latitude towards the poles, from ∼21—35 ppmv.

2. The abundance of H_2O shows some slight positive correlation with 1.74 μm radiance, increasing from ∼ 35 to 45 ppmv and remaining constant for radiances above 1×10^{-5} W/cm^2/μm/sr. There is little trend with latitude between the equator and -60°, but there is a sharp decrease in abundance from 40 to 20 ppmv between -60° and -75° latitude.

The trends observed in CO with latitude and radiance are the same as those presented in Tsang et al. (2008b) and Tsang et al. (2009). This serves to con-

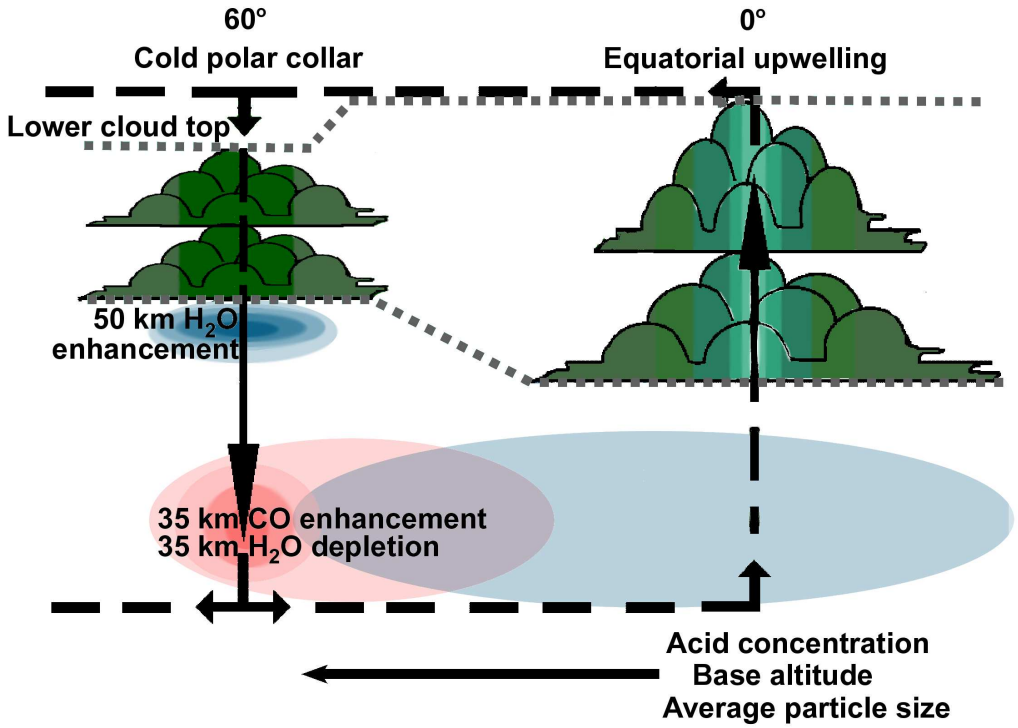

Figure 24: Variation of cloud properties with latitude.

firm the robustness of their result, as the same absolute values and trends are obtained after taking into account acid concentration and particle size variation. The H_2O abundance variation with radiance is over a similar range to that observed in Tsang et al. (2010) and Tsang et al. (2010, in preparation), but since those results were obtained assuming a 75 wt % sulphuric acid concentration the absolute values in this work are approximately 15 ppmv higher. This is consistent with the findings in Tsang et al. (2010, in preparation) that give retrieved abundances at 96 wt % sulphuric acid as 25 ppmv higher than those at 75 wt %. The average acid concentration measured in this work is between 85 and 90 wt %.

Tsang et al. (2008b) suggest that the increase in CO with latitude is due to the downwelling branch of the Hadley cell at -60° latitude drawing down CO-rich air from ∼65 km down to 35 km, followed by equatorward transport of this CO-rich air. This is consistent with our results, except that we do not see a peak at -60° latitude followed by a decrease closer to the poles. Instead, the peak seems to occur closer to -70°. However, we have few data beyond -75°, so any decreasing trend into the polar vortex would not be observed.

The sudden decrease in H_2O abundance with latitude may also be linked to Hadley circulation or downwelling, as the H_2O abundance is known to decrease with altitude on Venus. Drawing down of drier air could result in this trend. The slight positive correlation observed with 1.74 μm radiance, which corresponds to a negative correlation between H_2O abundance and cloud opacity, has been explored in more detail by Tsang et al. (2010) and Tsang et al. (2010, in preparation). It is expected that the correlation is due to water vapour from below the cloud layer being absorbed by the cloud in regions of upwelling as new condensational cloud is formed.

7 Assumptions and Sources of Uncertainty

7.1 Water Vapour

It can be seen from Figure 7 that there is sensitivity to water vapour at ∼25 km in the 1.74 μm radiance band. For the analysis in Section 5, we have assumed that the water vapour abundance at 25 km is 30 ppmv, as this is the consensus value quoted by Bézard & de Bergh (2007). The scatter on the results they present is 20—45 ppmv at this altitude. However, since the H_2O is allowed to vary in the 35—40 km altitude range, it is possible that some variation also occurs lower down in the atmosphere. This being the case, we might expect such variation to be coupled with that observed using the 2.4 μm band.

Taking this possibility into account prevents the use of the 2.2 μm to 1.74 μm band ratio to determine the acid concentration, since we are now allowing the radiance at 1.74 μm to vary due to the abundance of H_2O. It becomes necessary to find an alternative. If we assume that the variation in H_2O abundance at 25 km is coupled with the 35 km variation, which is reasonable in a well-mixed troposphere, then the ratio of the radiances at 2.4 μm and 1.74 μm will not be sensitive to any variation in H_2O abundance. There is sensitivity to mode 3 relative abundance and CO abundance, but the acid concentration is by far the biggest mode of variability. Two calculations of acid concentration using this ratio have been completed - the first, using the previously calculated values for CO abundance and mode 3 relative abundance, and the second assuming that these do not vary. The results are presented in Figure 25 with the results obtained using the original method outlined in Section 5.

It can be seen from Figure 25 that the variation in acid concentration is still required, although the magnitude of the variation is somewhat reduced in the two test cases. A final test case was to use the original 2.2:1.74 μm ratio

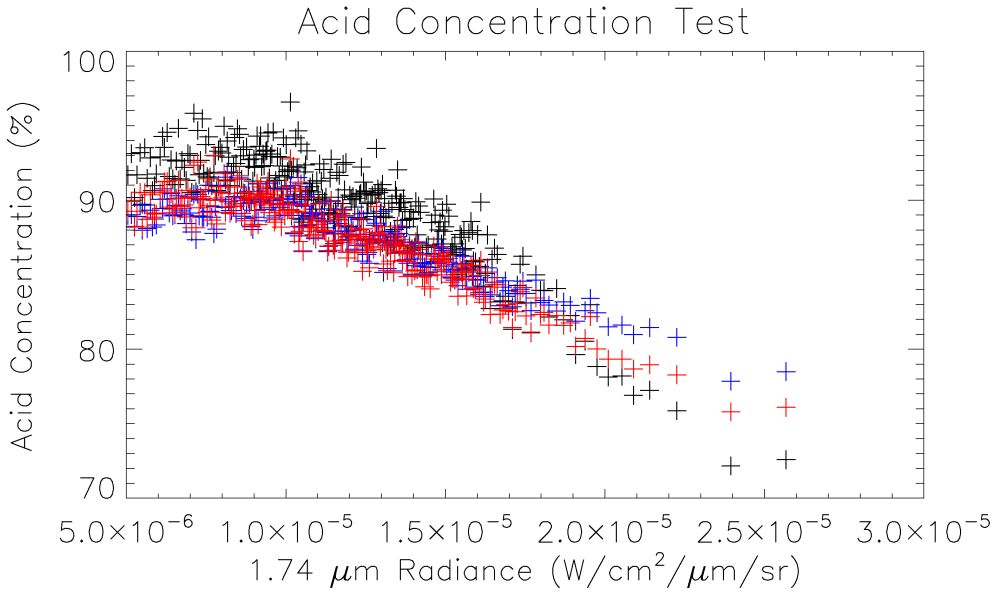

Figure 25: Tests determining the acid concentration whilst allowing coupled H_2O variations between 25 and 35 km. The black points are the original acid values, averaged once as in Figure 15. Red points correct for previously-determined values of CO and mode 3 relative abundance, and use the 2.4:1.74 μm ratio to calculate the acid concentration. Blue points are the same as the red points, but assume no variation in CO or mode 3 abundances.

to determine the acid concentration again, except that first a correction for the calculated water vapour abundance was applied to the 1.74 μm radiances. The results of this are shown in Figure 26.

It can be seen from these tests that the qualitative correlation of acid concentration with 1.74 μm radiance remains, even after allowing for variation in H_2O vapour at 25 km that is coupled with the variation at 35 km. The values obtained using the 2.4:1.74 μm ratio show a smaller spread than the original calculations (Figure 25), whilst the values obtained using the 2.2:1.74 μm ratio, after correcting for water, show a similar spread but are a few ppmv lower than the original values. However, the differences are small compared with the spread of values, so whilst this is a potential source of uncertainty it does not suggest that the conclusions of this work are invalid.

One further test is to examine the possibility of allowing uncoupled variation in H_2O vapour at 25 km to account for the variation present in the 2.2:1.74 μm ratio, instead of variation in acid concentration. The spread of values required, assuming an 85% acid concentration, is 0—80 ppmv, anti-

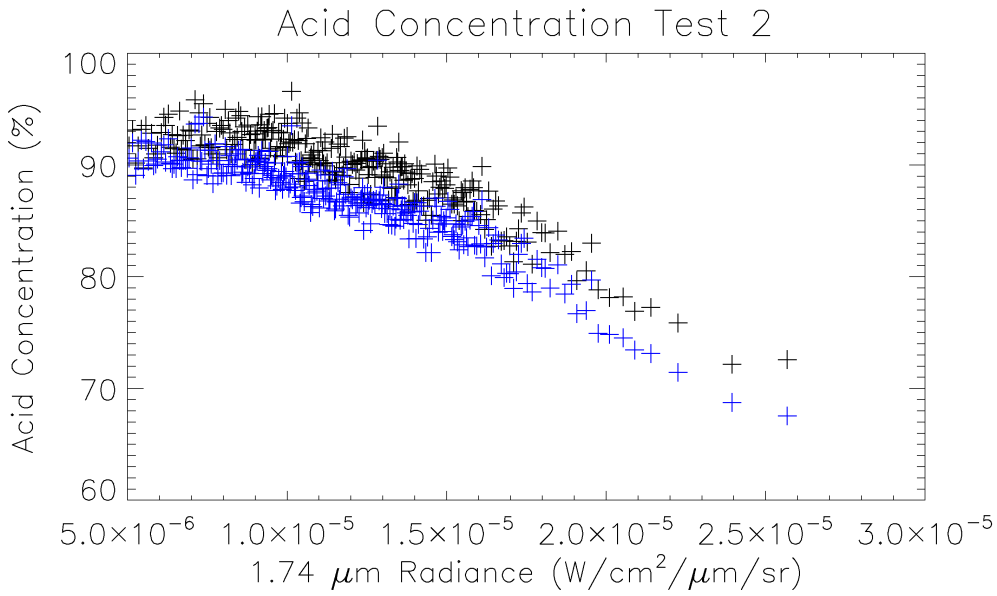

Figure 26: Comparison of acid concentrations obtained using the original method (black points) and after correction for calculated water vapour abundances (blue points). Averaging as in Figure 25.

correlated with the variation at 35 km. This is unlikely, since the spread of previously observed values is between 20 and 45 ppmv (Bézard & de Bergh 2007), and a mechanism for such extreme variation between 25 and 35 km in the well-mixed Venusian troposphere would be hard to justify. This scenario is sufficiently improbable that it can be ruled out.

A similar assumption has been made in the determination of the base altitude. It can be seen from Figure 7 that there is sensitivity to H_2O vapour at 50 km in the region between 2.5 and 2.6 μm. This band is centred slightly longwards of the 2.53 μm band used in the base altitude determination, but still affects this wavelength. We have assumed that the abundance of H_2O at 50 km is coupled with that at 35 km, since this results in the 2.53:2.4 μm ratio being independent of H_2O. However, this assumption may not be valid.

The centre of the H_2O absorption band is at around 2.56 μm, so whilst the 2.53 μm radiance is affected by this these two radiances could in theory be used as an indicator of the H_2O vapour abundance at 50 km. This has not been attempted previously as the radiances in this band are low, and are therefore likely to be significantly affected by noise and the odd-even effect (see Cardesin et al. (2008) for a description of the odd-even effect). However, the extraction of trends in radiance and latitude in this work involves aver-

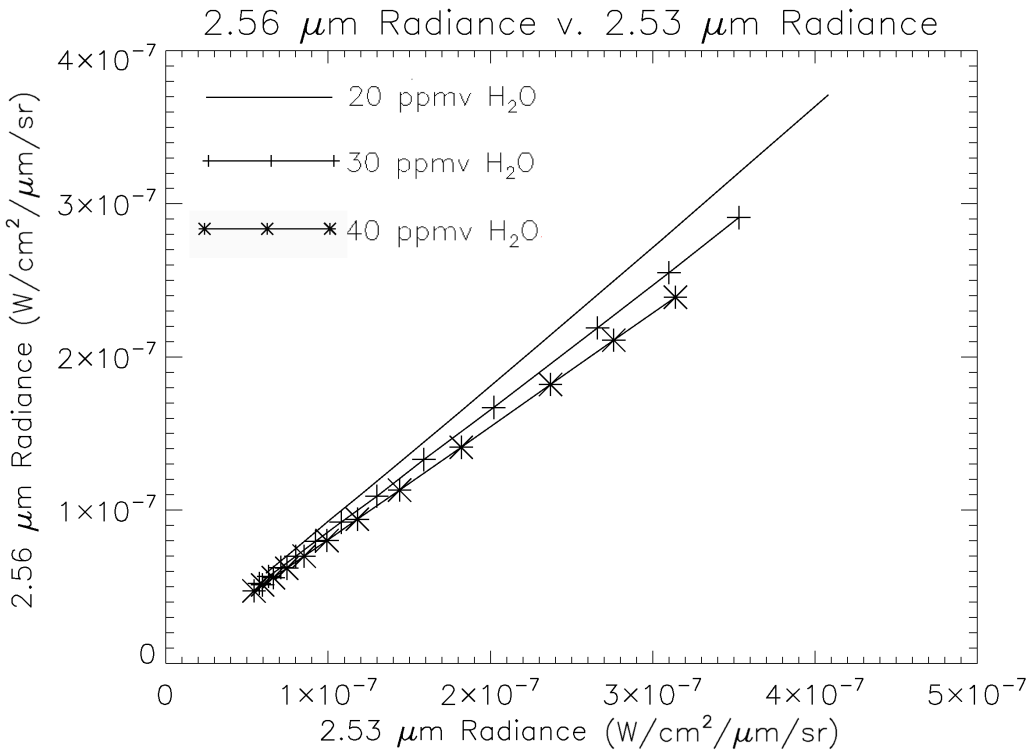

Figure 27: Model branches for 2.56 against 2.53 microns. There is no variation in this ratio due to particle size, acid concentration, base altitude or CO abundance. The different linestyles correspond to different water vapour abundances.

aging data from several different observations, and the radiances at 2.56 have been smoothed by a triangular filter as described in Section 5.2. This averaging increases the chances of obtaining a reliable measurement of the water vapour within the cloud, despite the limitations of the VIRTIS-M spectral resolution.

The dependence of this ratio on water vapour at 50 km is shown in Figure 27. The same method as outlined in Section 5 has been applied to this ratio for the collated low- to mid-latitude data from Table 4 and the collated data across all latitudes from Table 5. Since the water vapour abundance at 50 km affects the base altitude obtained using the 2.53:2.4 μm ratio, a correction for this has been applied and new base altitudes calculated. The new results for the radiance dependence are shown in Figures 28 and 29. The new results for latitudinal dependence are shown in Figure 30.

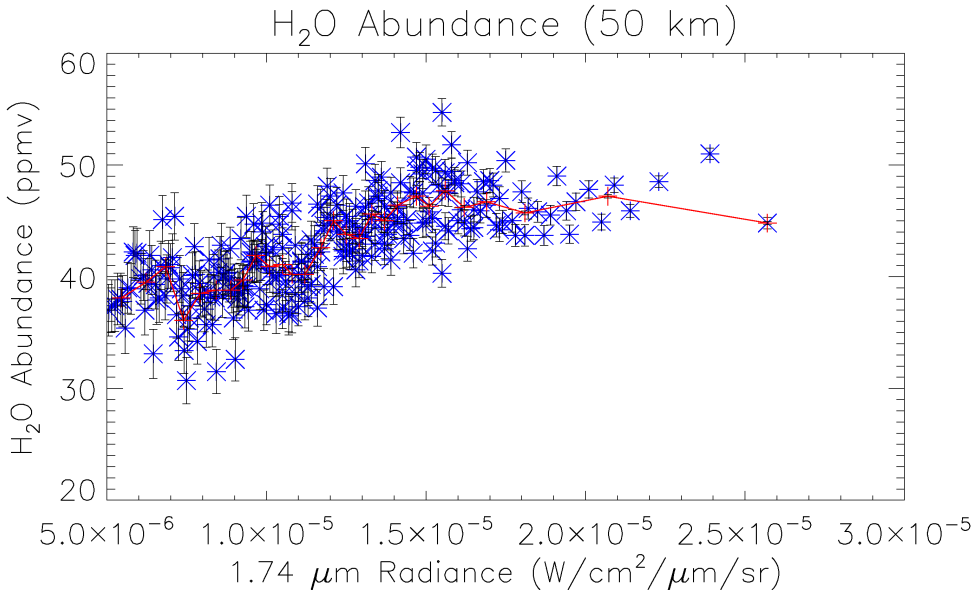

Figure 28: Variation of water vapour abundance at 50 km with radiance. Coadding is as in Figure 15.

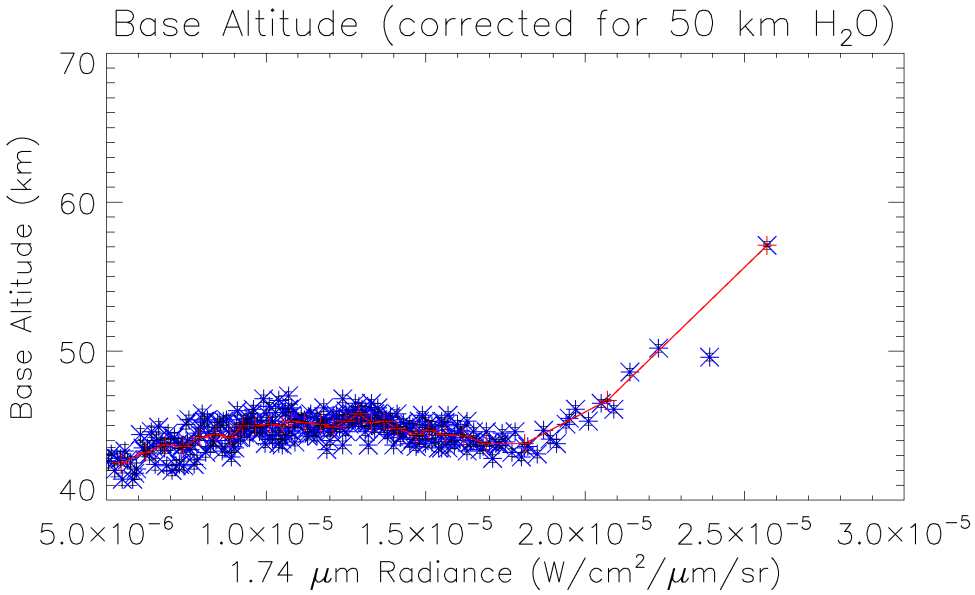

Figure 29: Modified variation of base altitude with radiance. Values are slightly lower than in Figure 16. Coadding is as in Figure 15.

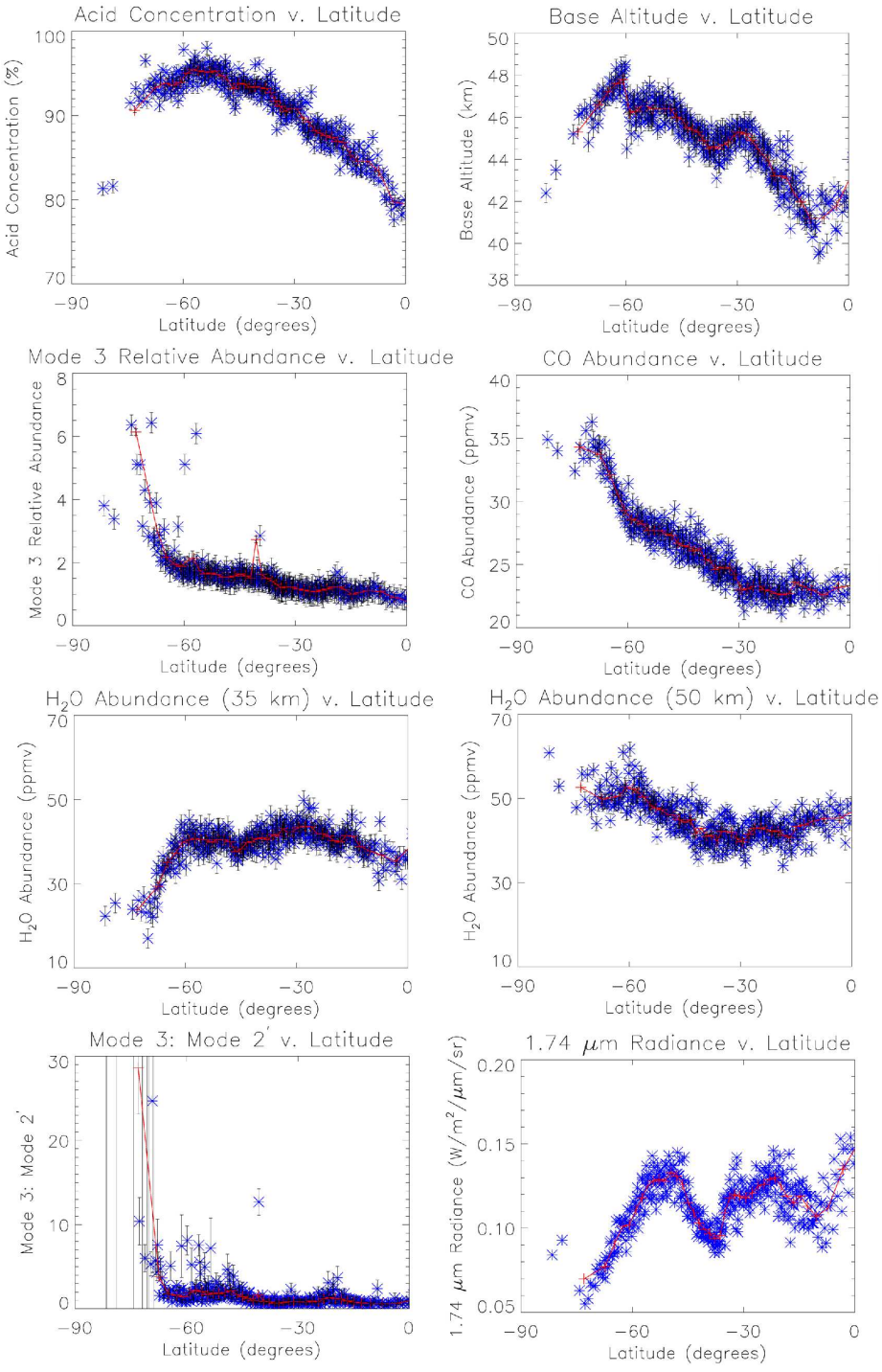

Figure 30: Collated final results for latitudinal variation, including mode 3 : mode 2′ ratio, 50 km H_2O and corrected base altitude.

7.2 Particle Size Distribution

Any conclusion arrived at using radiative transfer modelling techniques is of course dependent on the model parameters chosen. Several of these parameters have been independently constrained using this method, but a major variable that has been assumed to be constant is the mean radius of the mode 3 particles. The radius used here (see Table 3) has been taken from Pollack et al. (1993) and their selection of this number was based on the cumulative data from Pioneer Venus, Venera and ground-based observations. It is also the same as that used by Crisp (1986). However, it can be seen from Esposito et al. (1983) that great uncertainty about the precise nature of the mode 3 particles remained after analysis of the Pioneer Venus descent probe data – in particular, the size and aspect ratio were called into question. There was a discrepancy between measurements by the Pioneer Venus LCPS instrument, which identified a distinct distribution of larger particles, and nephelometer backscatter data which could not have been generated by particles with this size distribution and expected refractive indices. The LCPS size distributions did not yield the same optical depths as those measured by LSFR, if the particles were assumed to be spherical. There were also internal inconsistencies in the LCPS data, as overlapping size ranges gave conflicting measurements. The hypotheses suggested by Esposito et al. (1983) were that either the mode 3 particles were non-spherical, solid particles of unknown composition, or that the particles identified as a separate larger size mode were a misidentified tail of the mode 2 distribution. However, it seems certain that the Venusian atmosphere contains some large particles, with average diameters of 7—8 μm reported by Esposito et al. (1983), closely corresponding to our chosen effective radius of 3.65 μm.

Due to these uncertainties, it is important that we consider the implications of changing this effective radius r_{eff}, and especially any effect it might have on the analysis in this work. A branch plot showing the 2.2:1.74 μm ratio for different mode 3 effective radii is given in Figure 31. It can be seen first of all that the effective radius has a significant effect on this ratio, but also that the effect is highly non-linear. Most importantly, this ratio could not be used to determine the effective radius even assuming constant acid concentration, since finding a single-valued function to describe the variation is impossible as branches for $r_{eff} = 2.5\mu$m and $r_{eff} = 5\mu$m both lie above the branch for r_{eff}=3.65 μm on the plot.

This ratio becomes sensitive to the number of mode 3 particles if the effective radius is changed. The reason for this becomes apparent if the effect on the extinction cross-section is examined. It can be seen in Figure 32 that the extinction cross-section is almost zero at 2.2 μm for the nominal r_{eff},

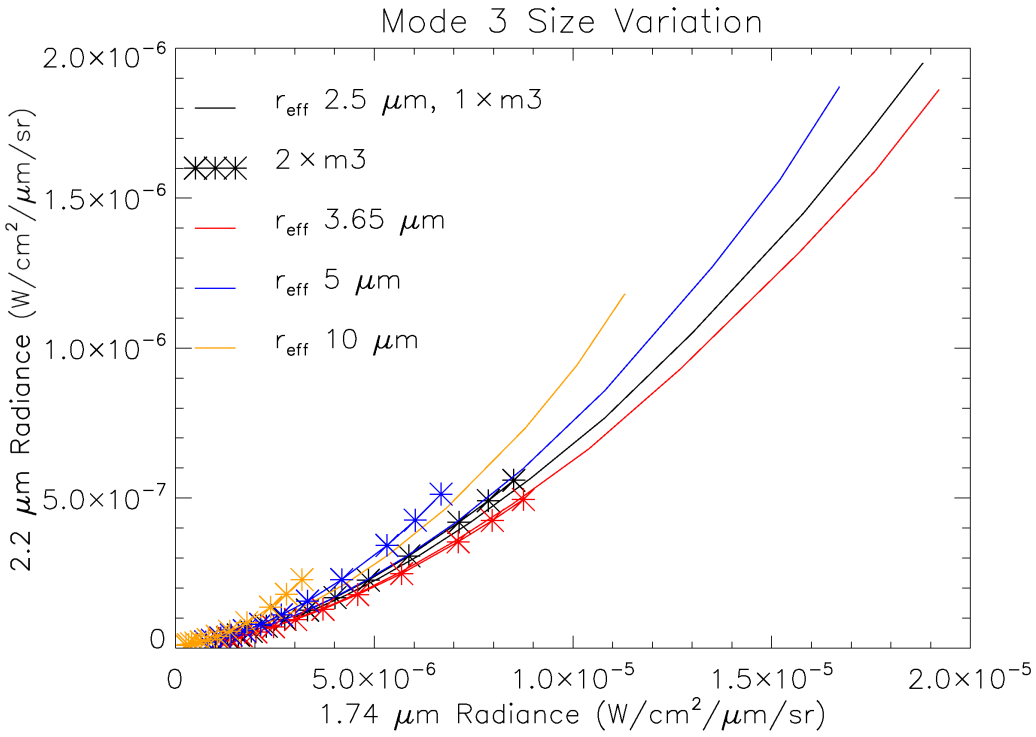

Figure 31: Changes in the 2.2:1.74 μm ratio with mode 3 effective radius. This has a significant, non-linear effect. The ratio also becomes sensitive to the number of mode 3 particles present for new values of r_{eff}.

but is non-zero for $r_{eff} = 10\mu$m. It is the small extinction cross-section at 2.2 μm for the nominal case that leads to this ratio having little dependence on the number of mode 3 particles.

We can perform one further test to justify our preference of the acid concentration hypothesis. The ratio between 2.4 and 2.32 μm remains relatively insensitive to the effective radius of mode 3, whilst retaining sensitivity to acid concentration. This ratio is then dependent on the abundances of H_2O and CO, number of mode 3 particles and acid concentration. We can independently determine the abundance of H_2O at 50 km, and it is reasonable to assume that this remains constant down to 35 km. We therefore use this to constrain the water vapour abundance. The CO abundance can also be determined independently of other quantities. The mode 3 abundance we assume to be as previously derived. We can then easily determine the acid concentration. A slight increase in acid concentration with decreasing radius is still observed (Figure 33), further supporting this hypothesis, although the

range of variation has decreased and there is significant scatter.

Changing the effective radius of mode 3 particles has an effect on derived mode 3 abundances and base altitudes, and these effects must be tested. Results of these tests are shown in Figures 34 and 35. It can be seen that increasing the radius to 5 μm reduces the calculated number of mode 3 particles, although a further increase to 10 μm increases the number again slightly. The calculated base altitude increases as the size increases. This is probably because fewer particles are required in the lower cloud, since the particles present in the lower cloud are comparatively larger and therefore more absorbing.

The introduction of this extra mode of uncertainty into the problem provides alternative possibilities for explaining the spectral behaviour of the Venusian cloud. The mode 3 effective radius cannot be independently constrained using VIRTIS, indeed to do so would probably require future in-situ measurements using descent probes or balloon platforms. However, our best estimate effective radius of 3.65 μm is well-supported by previous data analysis and modelling work (Crisp 1986, Pollack et al. 1993, McGouldrick & Toon 2008). The McGouldrick & Toon (2008) study in particular is significant, as the results of this microphysical model show effective radii for a single-mode cloud of no more than 4.5 μm, which is consistent with our choice of 3.65 μm for the nominal modal radius of mode 3.

7.3 Linearity and Acid Variation

I have assumed that the spectral variation due to alteration in the acid concentration is linear. This is not in reality the case, although the assumption is reasonable if values are close to 85 and 96%. If values for 75% are included in a 2.2:1.74 μm branch plot (Figure 36), it can be seen that the assumption of linearity breaks down. Unfortunately, the lack of data outside this range makes further characterisation of this non-linearity difficult. An easily-invertible numerical relationship between position on the branch plot and acid concentration is impossible to construct if model data for 75% is included. The assumption of linearity has therefore been retained, since the acid concentration values included are only intended to determine variation, rather than a measurement of absolute values. Also, the errors on the refractive index data from Palmer & Williams (1975) are not explicitly stated, but given the small values of the imaginary refractive index in the wavelength range of interest the percentage error is likely to be significant. Therefore, the assumption of linearity is unlikely to introduce significant further error.

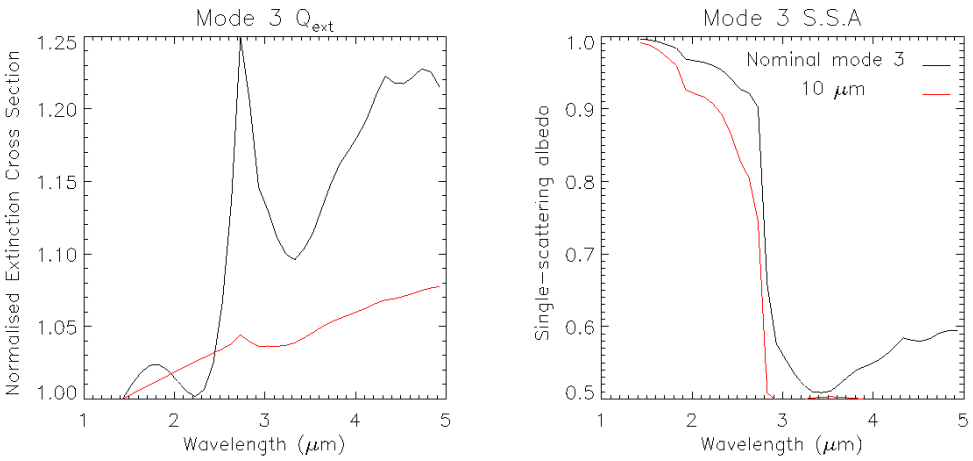

Figure 32: A comparison of extinction cross-section and single-scattering albedo generated for two different modal sizes for mode 3 particles. Increasing the particle size changes the absorption and scattering due to these particles as a function of wavelength.

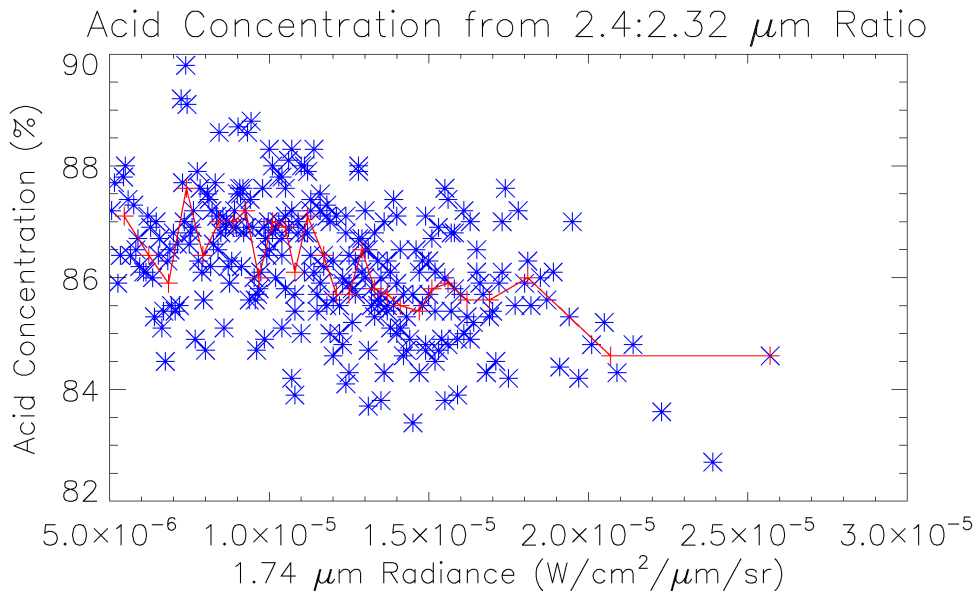

Figure 33: Acid concentration as calculated using the 2.4:2.32 µm ratio, using independently-calculated values for CO and H_2O, and previous results for mode 3 abundance.

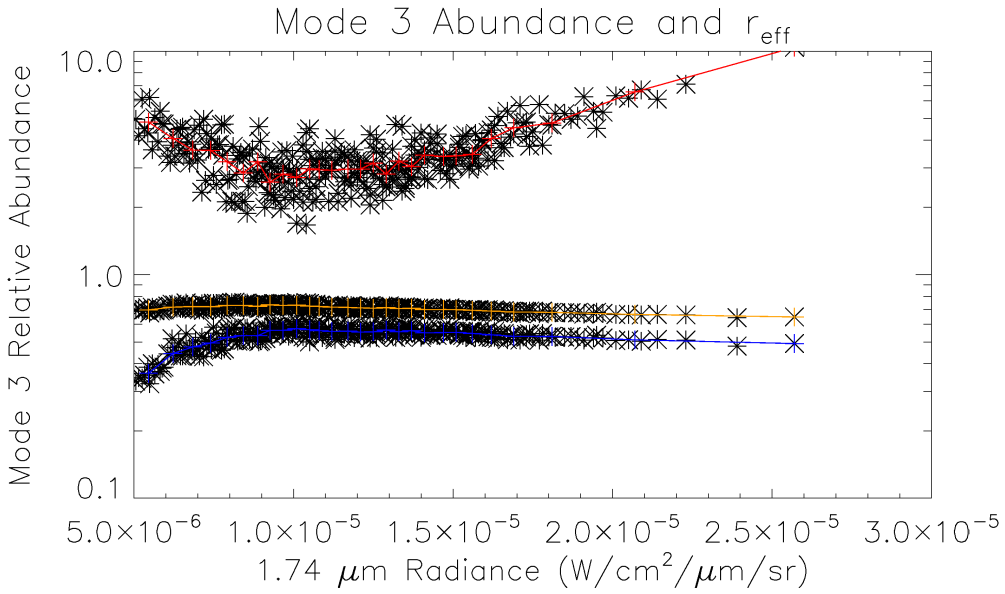

Figure 34: The effect of changing the mode 3 effective radius on the calculated relative abundance of mode 3 particles. 3.65μm results are in red, 5 μm in blue, 10 μm in orange. No acid concentration variation has been assumed.

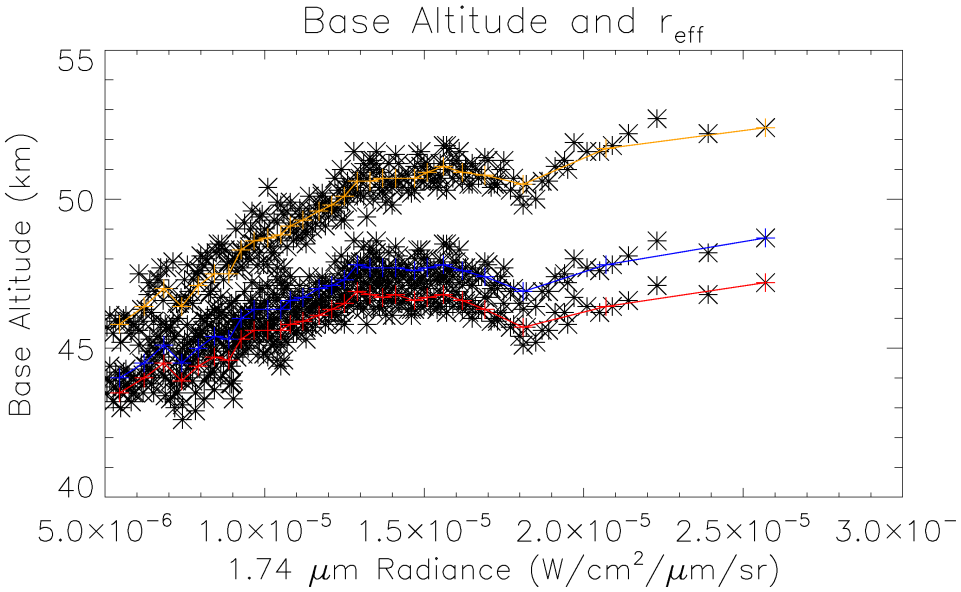

Figure 35: The effect of changing the mode 3 effective radius on the calculated base altitude. Colours are as above. No acid concentration variation has been assumed.

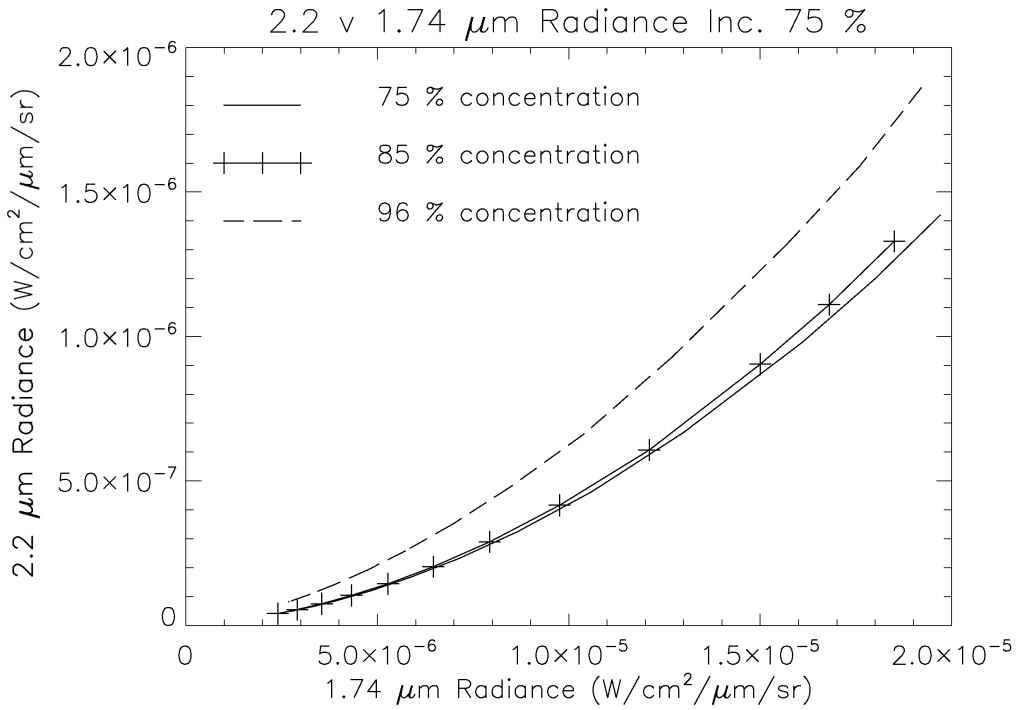

Figure 36: The 2.2 v. 1.74 μm branch plot with data for 75% added.

8 Future Work

8.1 Summary

The Venusian cloud still requires significant further study before a comprehensive understanding is achieved. The variations with radiance and position on the planet provide important clues about dynamical and chemical processes on Venus. The cloud also plays a significant role in the radiative balance of Venus. An improved understanding of the cloud enables the creation of models which better represent the current atmosphere of Venus, and may also lead to an improved understanding of the coupling of the clouds with the other atmospheric constituents, dynamics and geology of Venus. This new cloud parameterisation will therefore have implications not just for radiative transfer modelling of Venus but also for dynamical modelling, microphysical cloud modelling, studies of volcanism and evolutionary modelling. The main goals of this research are to:

1. Derive a new cloud model that provides the best possible representation of the meridional and vertical distribution of the cloud,

based on data from the VIRTIS instrument, and relate this if possible to global-scale dynamics.

2. Examine mesoscale departures from the above distribution and look for relationships with similar variations in gaseous abundances.

This work has so far generated a series of estimated correlations between acid concentration, average particle size, base altitude, CO and water vapour, against 1.74 μm radiance and latitude. In order to fully exploit the available data, the sensitivity of the shorter wavelength window regions at 1.31, 1.51 and 1.55 microns will be investigated. If these windows prove sensitive to changes in model cloud parameters, they will be used to provide estimated best-fit values for model parameters using the techniques already applied to the 1.74 and 2.3 micron windows. Once these regions are studied, all the infrared window regions with significant sensitivity to the cloud will have been investigated.

A brief study was conducted to determine whether high resolution data from VIRTIS-H might provide the means of distinguishing between the broad spectral effects of changing acid concentration and the narrower water vapour absorption. However, we find that the spectral resolution of VIRTIS-H is still insufficient to make this distinction, and this line of study will not be pursued as it is unlikely to be useful.

So far, data from only 15 observations have been analysed. Hundreds of suitable VIRTIS-M-IR observations exist, and a full coverage of the nightside southern hemisphere will be gained by extending the analysis to include all of these.

New, more comprehensive measurements of Venusian temperature profiles (Tellmann et al. 2009) and sulphuric acid refractive properties (Carlson & Anderson 2010) have been recently completed, and are likely to be made available for use in the near future. Contact is being maintained with these authors to follow their progress. These data will be used, if made available on time, as model inputs to improve the accuracy of the method over all southern hemisphere latitudes and a wider range of acid concentrations. Initial studies using new Venus temperature profiles have already been undertaken.

HITEMP (Rothman et al. 2010) is the current spectral database used to calculate CO_2 absorption parameters in the radiative transfer model. A specific database for CO_2, the Carbon Dioxide Spectroscopic Databank (CDSD), contains weak CO_2 lines that may make a difference to absorption at Venusian atmospheric temperatures. Recalculating forward models using line data from CDSD may improve model fits. Test spectra will be calculated and compared with the current spectra to decide whether the CDSD data greatly improves the accuracy of the calculations.

A theoretical limb darkening correction has been applied to the data processed in this work. Since such correction becomes significant at high emission angles, it is important to ensure that the correction is representative of the observed limb darkening in the VIRTIS dataset, and further refinement of the correction may be required. Tests and comparisons with other suggested corrections (Carlson et al. 1993, Longobardo et al. 2010) will be used to decide whether such refinement is necessary.

The shorter wavelength part of the VIRTIS-M-IR spectrum, between 1.0 and 1.25 microns, is used to study the surface. However, radiation from the surface must still pass through the cloud layer. Many analyses of these wavelengths assume that cloud parameters are constant over the region of interest (Hashimoto & Sugita 2003, Helbert et al. 2008). Investigating the effect of different cloud parameterisations on model spectra at these wavelengths would have an impact on surface parameters derived using such data. This may facilitate greater accuracy for such studies in the future, and as such will be a useful study should time permit.

8.2 Chronology

June 10—October 10

1. To extend the analysis described in this work to include the 1.31/1.51/1.55 micron window regions, and all suitable VIRTIS-M-IR dataset.

2. To write up the work presented here as a paper for the Icarus Venus special issue.

3. To verify model results using these windows and the 1.74/2.3 micron windows, then to examine possibilities for new constraints - especially sub-cloud haze and water vapour abundance at 25 km.

4. To investigate the effect of limb darkening corrections on the results and refine the correction if necessary.

5. To test the effect of including new temperature profiles (Tellmann et al. 2009) and CDSD line data and include them in the analysis if appropriate.

November 10—March 11

1. To include new sulphuric acid refractive index measurements from Carlson & Anderson (2010) (if available) and update results accordingly.

2. To finalise new constraints on acid concentration, average particle size, base altitude and abundances of CO and H_2O, including any for limb darkening and temperature structure that are deemed necessary following tests. This will involve checking that the results and method are self-consistent, confirming error margins and discussing the results in the light of previous measurements/physical constraints.

3. To obtain a final characterisation of the cloud variation with radiance and latitude, and to consider physical explanations for any observed correlations.

April 11—September 11

1. To investigate local deviations from the derived global trends.

2. To consider other possible modes of variability that can't be constrained with the existing data, including the presence of impurities in the cloud particles, changes in the effective radius of large particles, and changes in the cloud scale height, and where possible to model and discuss the effects of such changes.

3. To investigate the effect of different cloud parameterisations on the windows between 1.0 and 1.25 microns that are used to study the surface, and investigate the effect on retrieved surface temperature and emissivity variations, for example the results presented by Smrekar et al. (2010).

4. To write up the work and submit.

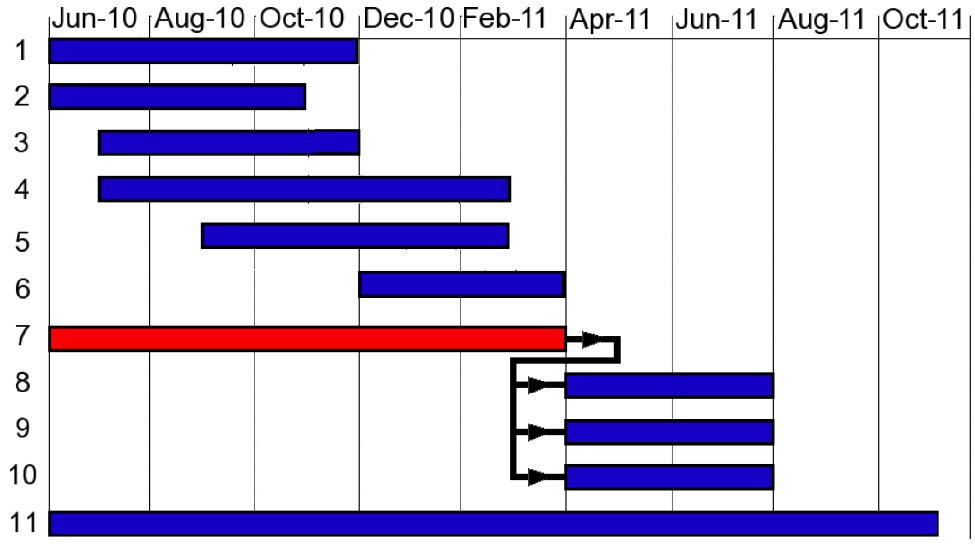

1. Investigate modes of variability that can be looked at using 1.31/1.51/1.55 micron windows
2. Write Icarus special issue paper
3. Verify existing model results from these windows and 1.74/2.3 μm windows
4. Test effects of limb darkening, temperature structure corrections and CDSD data
5. New constraints from 1.31/1.51/1.55 micron windows
6. Include new sulphuric acid refractive index measurements
7. Final characterisation of cloud with radiance and latitude
8. Investigation of local deviations from derived global trends
9. Consideration of other variables that can't be constrained with available methods/data
10. Investigation of the effect of different cloud models on surface windows (optional)
11. Write up

Figure 37: Gantt chart describing the intended progress of my future work.

References

Allen, D. A. & Crawford, J. W. (1984), 'Cloud Structure on the Dark Side of Venus', *Nature* **307**, 222–224.

Bézard, B. & de Bergh, C. (2007), 'Composition of the atmosphere of Venus below the clouds', *Journal of Geophysical Research (Planets)* **112**(E04S07).

Bullock, M. A. (1997), The Stability of Climate on Venus, PhD thesis, University of Colorado, Boulder, Colorado.

Cardesin, A., Erard, S. & Piccioni, G. (2008), *VIRTIS-M Calibration Document*.

Carlson, R. W. & Anderson, M. S. (2010), Near-Infrared Optical Constants of Sulphuric Acid, *in* 'International Venus Conference Aussois 2010 Book of Abstracts', p. 79.

Carlson, R. W., Kamp, L. W., Baines, K. H., Pollack, J. B., Grinspoon, D. H., Encrenaz, T., Drossart, P. & Taylor, F. W. (1993), 'Variations in Venus cloud particle properties: A new view of Venus's cloud morphology as observed by Galileo Near-Infrared Mapping Spectrometer', *Planetary and Space Science* **41**, 477–485.

Cimino, J. (1982), 'The composition and vertical structure of the lower cloud deck on Venus', *Icarus* **51**, 334–357.

Colin, L. (1980), 'The Pioneer Venus Program', *Journal of Geophysical Research* **85**, 7575–7598.

Coradini, A., Capaccioni, F., Drossart, P., Semery, A., Arnold, G. & Schade, U. (1999), 'VIRTIS: The imaging spectrometer of the Rosetta mission', *Advances in Space Research* **24**, 1095–1104.

Coradini, A., Capaccioni, F., Drossart, P., Semery, A., Arnold, G., Schade, U., Angrilli, F., Barucci, M. A., Bellucci, G., Bianchini, G., Bibring, J. P., Blanco, A., Blecka, M., Bockelee-Morvan, D., Bonsignori, R., Bouye, M., Bussoletti, E., Capria, M. T., Carlson, R., Carsenty, U., Cerroni, P., Colangeli, L., Combes, M., Combi, M., Crovisier, J., Dami, M., DeSanctis, M. C., DiLellis, A. M., Dotto, E., Encrenaz, T., Epifani, E., Erard, S., Espinasse, S., Fave, A., Federico, C., Fink, U., Fonti, S., Formisano, V., Hello, Y., Hirsch, H., Huntzinger, G., Knoll, R., Kouach, D., Ip, W. H., Irwin, P., Kachlicki, J., Langevin, Y., Magni,

G., McCord, T., Mennella, V., Michaelis, H., Mondello, G., Mottola, S., Neukum, G., Orofino, V., Orosei, R., Palumbo, P., Peter, G., Pforte, B., Piccioni, G., Reess, J. M., Ress, E., Saggin, B., Schmitt, B., Stefanovitch, Stern, A., Taylor, F., Tiphene, D. & Tozzi, G. (1998), 'Virtis : an imaging spectrometer for the rosetta mission', *Planetary and Space Science* **46**, 1291–1304.

Crisp, D. (1986), 'Radiative forcing of the Venus mesosphere. I - Solar fluxes and heating rates', *Icarus* **67**, 484–514.

Donahue, T. M., Hoffman, J. H., Hodges, R. R. & Watson, A. J. (1982), 'Venus was wet - A measurement of the ratio of deuterium to hydrogen', *Science* **216**, 630–633.

Drossart, P., Piccioni, G., Adriani, A., Angrilli, F., Arnold, G., Baines, K. H., Bellucci, G., Benkhoff, J., Bézard, B., Bibring, J.-P., Blanco, A., Blecka, M. I., Carlson, R. W., Coradini, A., di Lellis, A., Encrenaz, T., Erard, S., Fonti, S., Formisano, V., Fouchet, T., Garcia, R., Haus, R., Helbert, J., Ignatiev, N. I., Irwin, P. G. J., Langevin, Y., Lebonnois, S., Lopez-Valverde, M. A., Luz, D., Marinangeli, L., Orofino, V., Rodin, A. V., Roos-Serote, M. C., Saggin, B., Sanchez-Lavega, A., Stam, D. M., Taylor, F. W., Titov, D., Visconti, G., Zambelli, M., Hueso, R., Tsang, C. C. C., Wilson, C. F. & Afanasenko, T. Z. (2007), 'Scientific goals for the observation of Venus by VIRTIS on ESA/Venus express mission', *Planetary and Space Science* **55**, 1653–1672.

Erard, S., Drossart, P. & Piccioni, G. (2009), 'Multivariate analysis of Visible and Infrared Thermal Imaging Spectrometer (VIRTIS) Venus Express nightside and limb observations', *Journal of Geophysical Research (Planets)* **114**(E13).

Esposito, L. W., Copley, M., Eckert, R., Gates, L., Stewart, A. I. F. & Worden, H. (1988), 'Sulfur dioxide at the Venus cloud tops, 1978-1986', *Journal of Geophysical Research* **93**, 5267–5276.

Esposito, L. W., Knollenberg, R. G., Marov, M. I., Toon, O. B. & Turco, R. P. (1983), *The clouds and hazes of Venus*, The University of Arizona, pp. 484–564.

Grinspoon, D. H., Pollack, J. B., Sitton, B. R., Carlson, R. W., Kamp, L. W., Baines, K. H., Encrenaz, T. & Taylor, F. W. (1993), 'Probing Venus's cloud structure with Galileo NIMS', *Planetary and Space Science* **41**, 515–542.

Hashimoto, G. L. & Sugita, S. (2003), 'On observing the compositional variability of the surface of Venus using nightside near-infrared thermal radiation', *Journal of Geophysical Research (Planets)* **108**(E9), 5109.

Head, III, J. W., Crumpler, L. S. & Aubele, J. C. (1992), 'Venus volcanism: A global overview from Magellan data', *LPI Contributions* **789**, 43–45.

Helbert, J., Müller, N., Kostama, P., Marinangeli, L., Piccioni, G. & Drossart, P. (2008), 'Surface brightness variations seen by VIRTIS on Venus Express and implications for the evolution of the Lada Terra region, Venus', *Geophysical Research Letters* **35**(L11201).

Houze, Jr., R. A. (1993), *Cloud Dynamics*, Academic Press.

Imamura, T. & Hashimoto, G. L. (2002), 'H_2SO_4 cycle in the Venusian tropical atmosphere as constrained by a microphysical cloud model', *Advances in Space Research* **29**, 249–254.

Irwin, P. G. J., Calcutt, S. B. & Taylor, F. W. (1997), 'Radiative transfer models for Galileo NIMS studies of the atmosphere of Jupiter', *Advances in Space Research* **19**, 1149–1158.

Irwin, P. G. J., Teanby, N. A., de Kok, R., Fletcher, L. N., Howett, C. J. A., Tsang, C. C. C., Wilson, C. F., Calcutt, S. B., Nixon, C. A. & Parrish, P. D. (2008), 'The NEMESIS planetary atmosphere radiative transfer and retrieval tool', *Journal of Quantitative Spectroscopy and Radiative Transfer* **109**, 1136–1150.

James, E. P., Toon, O. B. & Schubert, G. (1997), 'A Numerical Microphysical Model of the Condensational Venus Cloud', *Icarus* **129**, 147–171.

Kliore, A., Moroz, V. & G., K. (1986), *The Venus International Reference Atmosphere*, Pergamon Press, Oxford.

Knollenberg, R. G. & Hunten, D. M. (1980), 'The microphysics of the clouds of Venus - Results of the Pioneer Venus particle size spectrometer experiment', *Journal of Geophysical Research* **85**, 8039–8058.

Kolodner, M. A. & Steffes, P. G. (1998), 'The Microwave Absorption and Abundance of Sulfuric Acid Vapor in the Venus Atmosphere Based on New Laboratory Measurements', *Icarus* **132**, 151–169.

Krasnopolsky, V. A. (1989), 'VEGA Mission results and chemical composition of Venusian clouds', *Icarus* **80**, 202–210.

Lacis, A. A. & Oinas, V. (1991), 'A description of the correlated-k distribution method for modelling nongray gaseous absorption, thermal emission, and multiple scattering in vertically inhomogeneous atmospheres', *Journal of Geophysical Research* **96**, 9027–9064.

Longobardo, A., Palomba, E., Zinzi, A., G., P., Drossart, P. & The VIRTIS-VeX Team (2010), A novel approach for Limb Darkening Correction on Venus nightside NIR spectrum: results and implications, *in* 'International Venus Conference Aussois 2010 Book of Abstracts', p. 89.

Marcq, E., Bézard, B., Drossart, P., Piccioni, G., Reess, J. M. & Henry, F. (2008), 'A latitudinal survey of CO, OCS, H_2O, and SO_2 in the lower atmosphere of Venus: Spectroscopic studies using VIRTIS-H', *Journal of Geophysical Research (Planets)* **113**(E12).

Marcq, E., Encrenaz, T., Bézard, B. & Birlan, M. (2006), 'Remote sensing of Venus'lower atmosphere from ground-based IR spectroscopy: Latitudinal and vertical distribution of minor species', *Planetary and Space Science* **54**, 1360–1370.

McGouldrick, K. & Toon, O. B. (2007), 'An investigation of possible causes of the holes in the condensational Venus cloud using a microphysical cloud model with a radiative-dynamical feedback', *Icarus* **191**, 1–24.

McGouldrick, K. & Toon, O. B. (2008), 'Observable effects of convection and gravity waves on the Venus condensational cloud', *Planetary and Space Science* **56**, 1112–1131.

Palmer, K. F. & Williams, D. (1975), 'Optical constants of sulfuric acid: application to the clouds of Venus?', *Applied Optics* **14**, 208–219.

Piccialli, A., Titov, D. V., Grassi, D., Khatuntsev, I., Drossart, P., Piccioni, G. & Migliorini, A. (2008), 'Cyclostrophic winds from the Visible and Infrared Thermal Imaging Spectrometer temperature sounding: A preliminary analysis', *Journal of Geophysical Research (Planets)* **113**(E12).

Piccioni, G., Drossart, P., Sanchez-Lavega, A., Hueso, R., Taylor, F. W., Wilson, C. F., Grassi, D., Zasova, L., Moriconi, M., Adriani, A., Lebonnois, S., Coradini, A., Bézard, B., Angrilli, F., Arnold, G., Baines, K. H., Bellucci, G., Benkhoff, J., Bibring, J. P., Blanco, A., Blecka, M. I., Carlson, R. W., di Lellis, A., Encrenaz, T., Erard, S., Fonti, S., Formisano, V., Fouchet, T., Garcia, R., Haus, R., Helbert, J., Ignatiev, N. I., Irwin, P. G. J., Langevin, Y., Lopez-Valverde, M. A., Luz, D., Marinangeli,

L., Orofino, V., Rodin, A. V., Roos-Serote, M. C., Saggin, B., Stam, D. M., Titov, D., Visconti, G., Zambelli, M., Ammannito, E., Barbis, A., Berlin, R., Bettanini, C., Boccaccini, A., Bonnello, G., Bouye, M., Capaccioni, F., Cardesin Moinelo, A., Carraro, F., Cherubini, G., Cosi, M., Dami, M., de Nino, M., Del Vento, D., di Giampietro, M., Donati, A., Dupuis, O., Espinasse, S., Fabbri, A., Fave, A., Veltroni, I. F., Filacchione, G., Garceran, K., Ghomchi, Y., Giustini, M., Gondet, B., Hello, Y., Henry, F., Hofer, S., Huntzinger, G., Kachlicki, J., Knoll, R., Driss, K., Mazzoni, A., Melchiorri, R., Mondello, G., Monti, F., Neumann, C., Nuccilli, F., Parisot, J., Pasqui, C., Perferi, S., Peter, G., Piacentino, A., Pompei, C., Reess, J.-M., Rivet, J.-P., Romano, A., Russ, N., Santoni, M., Scarpelli, A., Semery, A., Soufflot, A., Stefanovitch, D., Suetta, E., Tarchi, F., Tonetti, N., Tosi, F. & Ulmer, B. (2007), 'South-polar features on Venus similar to those near the north pole', *Nature* **450**, 637–640.

Pollack, J. B., Erickson, E. F., Witteborn, F. C., Chackerian, Jr., C., Summers, A. L., van Camp, W., Baldwin, B. J., Augason, G. C. & Caroff, L. J. (1974), 'Aircraft observations of Venus' near-infrared reflection spectrum - Implications for cloud composition', *Icarus* **23**, 8–26.

Pollack, J., Dalton, J., Grinspoon, D., Wattson, R., Freedman, R., Crisp, D., Allen, D., Bézard, B., de Bergh, C. & Giver, L. (1993), 'Near-Infrared Light from Venus' Nightside: A Spectroscopic Analysis', *Icarus* **103**, 1–42.

Prinn, R. G. (1978), 'Venus - Chemistry of the lower atmosphere prior to the Pioneer Venus mission', *Geophysical Research Letters* **5**, 973–976.

Rogers, R. R. & Yau, M. K. (1989), *A Short Course in Cloud Physics*, third edn, Pergamon Press.

Rothman, L., Gordon, I., Barber, R., Dothe, H., Gamache, R., Goldman, A., Perevalov, V., Tashkun, S. & Tennyson, J. (2010), 'Hitemp, the high-temperature molecular spectroscopic database', *Journal of Quantitative Spectroscopy and Radiative Transfer* **In Press, Corrected Proof**.

Rothman, L. S., Barbe, A., Benner, D. C., Brown, L. R., Camy-Peyret, C., Carleer, M. R., Chance, K., Clerbaux, C., Dana, V., Devi, V. M., Fayt, A., Flaud, J. M., Gamache, R. R., Goldman, A., Jacquemart, D., Jucks, K. W., Lafferty, W. J., Mandin, J. Y., Massie, S. T., Nemtchinov, V., Newnham, D. A., Perrin, A., Rinsland, C. P., Schroeder, J., Smith, K. M., Smith, M. A. H., Tang, K., Toth, R. A., Auwera, J. V., Varanasi,

P. & Yoshino, K. (2003), 'The hitran molecular spectroscopic database: edition of 2000 including updates through 2001', *Journal of Quantitative Spectroscopy and Radiative Transfer* **82**(1-4), 5 – 44. The HITRAN Molecular Spectroscopic Database: Edition of 2000 Including Updates of 2001.

Sagan, C. (1960), 'The Surface Temperature of Venus.', *Astronomical Journal* **65**, 352–353.

Sagan, C. (1962), 'Structure of the lower atmosphere of Venus', *Icarus* **1**, 151–169.

Satoh, T., Imamura, T., Hashimoto, G. L., Iwagami, N., Mitsuyama, K., Sorahana, S., Drossart, P. & Piccioni, G. (2009), 'Cloud structure in Venus middle-to-lower atmosphere as inferred from VEX/VIRTIS 1.74 μm data', *Journal of Geophysical Research (Planets)* **114**(E13).

Saunders, R. S. & Malin, M. C. (1977), 'Geologic interpretation of new observations of the surface of Venus', *Geophysical Research Letters* **4**, 547–550.

Seiff, A., Schofield, J. T., Kliore, A. J., Taylor, F. W. & Limaye, S. S. (1985), 'Models of the structure of the atmosphere of Venus from the surface to 100 kilometers altitude', *Advances in Space Research* **5**, 3–58.

Smrekar, S. E., Stofan, E. R., Mueller, N., Treiman, A., Elkins-Tanton, L., Helbert, J., Piccioni, G. & Drossart, P. (2010), 'Recent Hotspot Volcanism on Venus from VIRTIS Emissivity Data', *Science* **328**, 605–608.

Svedhem, H., Titov, D. V., McCoy, D., Lebreton, J.-P., Barabash, S., Bertaux, J.-L., Drossart, P., Formisano, V., Häusler, B., Korablev, O., Markiewicz, W. J., Nevejans, D., Pätzold, M., Piccioni, G., Zhang, T. L., Taylor, F. W., Lellouch, E., Koschny, D., Witasse, O., Eggel, H., Warhaut, M., Accomazzo, A., Rodriguez-Canabal, J., Fabrega, J., Schirmann, T., Clochet, A. & Coradini, M. (2007), 'Venus Express—The first European mission to Venus', *Planetary and Space Science* **55**, 1636–1652.

Taylor, F. & Grinspoon, D. (2009), 'Climate evolution of Venus', *Journal of Geophysical Research (Planets)* **114**(E13).

Teanby, N. A., de Kok, R., Irwin, P. G. J., Osprey, S., Vinatier, S., Gierasch, P. J., Read, P. L., Flasar, F. M., Conrath, B. J., Achterberg, R. K., Bézard, B., Nixon, C. A. & Calcutt, S. B. (2008), 'Titan's winter polar

vortex structure revealed by chemical tracers', *Journal of Geophysical Research (Planets)* **113**(E12).

Tellmann, S., Pätzold, M., Häusler, B., Bird, M. K. & Tyler, G. L. (2009), 'Structure of the Venus neutral atmosphere as observed by the Radio Science experiment VeRa on Venus Express', *Journal of Geophysical Research (Planets)* **114**(E13).

Titov, D. V., Taylor, F. W., Svedhem, H., Ignatiev, N. I., Markiewicz, W. J., Piccioni, G. & Drossart, P. (2008), 'Atmospheric structure and dynamics as the cause of ultraviolet markings in the clouds of Venus', *Nature* **456**, 620–623.

Tsang, C. C. C. (2007), The Composition and Circulation of the Atmosphere of Venus using Venus Express/VIRTIS Data, PhD thesis, Atmospheric, Oceanic and Planetary Physics, Department of Physics University of Oxford.

Tsang, C. C. C., Irwin, P. G. J., Wilson, C. F., Taylor, F. W., Lee, C., de Kok, R., Drossart, P., Piccioni, G., Bezard, B. & Calcutt, S. (2008b), 'Tropospheric carbon monoxide concentrations and variability on Venus from Venus Express/VIRTIS-M observations', *Journal of Geophysical Research (Planets)* **113**(E12).

Tsang, C. C. C., Taylor, F. W., Wilson, C. F., Liddell, S. J., Irwin, P. G. J., Piccioni, G., Drossart, P. & Calcutt, S. B. (2009), 'Variability of CO concentrations in the Venus troposphere from Venus Express/VIRTIS using a Band Ratio Technique', *Icarus* **201**, 432–443.

Tsang, C. C. C., Wilson, C. F., Barstow, J. K., Irwin, P. G. J., Taylor, F. W., McGouldrick, K., Piccioni, G., Drossart, P. & Svedhem, H. (2010), 'Correlations between cloud thickness and sub-cloud water abundance on Venus', *Geophysical Research Letters* **37**(L02202).

Tsang, C. C. C., Wilson, C. F., Barstow, J. K., Irwin, P. G. J., Taylor, F. W., McGouldrick, K., Piccioni, G., Drossart, P. & Svedhem, H. (2010, in preparation), 'Venuss Subcloud Composition: A Comprehensive Study of the Retrieval of Water Vapour and Carbonyl Sulphide', *Icarus* **113**(E12).

Tsang, C., Irwin, P., Taylor, F. & Wilson, C. (2008a), 'A correlated-k model of radiative transfer in the near-infrared windows of venus', *Journal of Quantitative Spectroscopy and Radiative Transfer* **109**(6), 1118 – 1135. Spectroscopy and Radiative Transfer in Planetary Atmospheres.

Wilson, C. F., Guerlet, S., Irwin, P. G. J., Tsang, C. C. C., Taylor, F. W., Carlson, R. W., Drossart, P. & Piccioni, G. (2008), 'Evidence for anomalous cloud particles at the poles of Venus', *Journal of Geophysical Research (Planets)* **113**(E12).

Young, A. T. (1973), 'Are the Clouds of Venus Sulfuric Acid?', *Icarus* **18**, 564–582.

Zhang, T. L., Baumjohann, W., Delva, M., Auster, H.-U., Balogh, A., Russell, C. T., Barabash, S., Balikhin, M., Berghofer, G., Biernat, H. K., Lammer, H., Lichtenegger, H., Magnes, W., Nakamura, R., Penz, T., Schwingenschuh, K., Vörös, Z., Zambelli, W., Fornacon, K.-H., Glassmeier, K.-H., Richter, I., Carr, C., Kudela, K., Shi, J. K., Zhao, H., Motschmann, U. & Lebreton, J.-P. (2006), 'Magnetic field investigation of the Venus plasma environment: Expected new results from Venus Express', *Planetary and Space Science* **54**, 1336–1343.